9-9-2007

Compact modeling of neutron damage effects in a bipolar junction transistor

Teresa Gutierrez

Compact Modeling of Neutron Damage Effects in a Bipolar Junction Transistor

by

Teresa B. Gutierrez

B.S., Electrical Engineering, University of New Mexico, 1999

THESIS

Submitted in Partial Fulfillment of the

Requirements for the Degree of

Master of Science

Electrical Engineering

The University of New Mexico

Albuquerque, New Mexico

July 2007

Dedication

This work is dedicated to those who make this achievement worthwhile.

To my boyfriend, Steve, and his kids, Vaughan and Hannah.

To my parents, Rosalio and Gloria.

To my brother, Ken, and his family, Cyra, Jessi, and Kennedy.

And to my cousin, Nick.

Acknowledgments

First and foremost, I would like to thank my friend and colleague, Charles Hembree. Chuck has been instrumental in my accomplishments as a graduate student. His guidance and insight helped make this work valuable to the discipline of modeling and simulation of radiation effects on electronics.

I would like to thank my academic advisor, Dr. Charles F. Hawkins, and committee member, Dr. Mark A. Gilmore, for their involvement in my graduate study and review of this manuscript.

Finally, I would like to extend a special thank you to my colleagues at Sandia National Laboratories who provided assistance in this research, Steven K. Dunlap, Albert V. Nunez, and Eric R. Keiter.

Compact Modeling of Neutron Damage Effects in a Bipolar Junction Transistor

by

Teresa B. Gutierrez

ABSTRACT OF THESIS

Submitted in Partial Fulfillment of the
Requirements for the Degree of

Master of Science
Electrical Engineering

The University of New Mexico

Albuquerque, New Mexico

July 2007

Compact Modeling of Neutron Damage Effects in a Bipolar Junction Transistor

by

Teresa B. Gutierrez

B.S., Electrical Engineering, University of New Mexico, 1999

M.S., Electrical Engineering, University of New Mexico, 2007

Abstract

The performance of microelectronics in a radiation environment is an important concern for defense and space applications. Bipolar junction transistors (BJTs), in particular, are susceptible to neutron radiation. Neutron radiation affects BJT performance primarily by creating lattice defects, which can dramatically increase carrier recombination rate. In turn, the increase in recombination rate degrades the current gain. Two approaches were taken in the development of a compact BJT model that include the effects of static neutron damage. One approach is based on the Gummel-Poon term for recombination current. The other approach is based on the Shockley-Read-Hall theory of recombination. Simulation results of the BJT neutron-effects model compare favorably with measured data of BJT test structures. Application of the neutron-effects BJT model in a voltage reference circuit provides critical information for circuit design in a neutron environment.

Contents

List of Figures

List of Tables

Chapter 1

Introduction

The performance of microelectronics in radiation environments is an important concern for defense and space applications. To optimally design reliable integrated circuits and accurately predict detailed circuit performance, the influence of physical characteristics on the electrical characteristics of a device must be well understood in both normal and radiation environments. Furthermore, precise device models that include effects of radiation damage enable the designer to accomplish the circuit design over the full range of functional specifications. This research presents a device model for a bipolar junction transistor (BJT) that includes the effects of damage caused by neutron radiation. Thus, the model is intended to help design and study circuits in a fast neutron environment.

Chapter 1 includes fundamental physics of semiconductor devices as well as a discussion on the damage effects in silicon devices caused by neutrons. Chapter 2 provides device characterization of BJT test structures for a given process, which includes fabrication and testing. Chapter 3 describes the Gummel-Poon BJT model, which serves as a basis for the neturon-effects BJT model. It also presents the development of the neutron-effects BJT model. An application of the model is presented in Chapter 4. Chapter 5 summarizes the research and discusses future work.

1.1 Physics of Semiconductor Devices

This section describes basic concepts of solid-state physics in semiconductor material and devices. Although the concepts can be applied to all semiconductor materials, silicon is the primary source for modern electronic systems. A description of pertinent properties of silicon provides a foundation for understanding basic physical structure, applied electrical bias, and signal voltages and currents of microelectronic devices. Comprehension of these concepts is important for investigating damage effects of neutron radiation to develop device models.

A full treatment of device physics usually begins with derivations of carrier densities in the semiconductor material of interest. The interactions of the carriers with the material (i.e. masses, mobilities) are a function of the material's band structure. The addition of electric fields and carrier gradients requires the Boltzman transport theory, which is usually reduced to a drift-diffusion treatment to describe carrier movements. Impurities such as dopants influence the band structure to second order, but more importantly, the electric fields and carrier densities are influenced to first order. Regions of rapid spatially changing impurity concentrations give rise to devices such as *pn* junctions. Thus, the first step in analyzing these devices is to begin with the simplest drift-diffusion description, the continuity equation.

1.1.1 Continuity Equation

Current in a semiconductor is due to the movement of carriers. The current density for electrons and holes due to the drift-diffusion mechanisms are described by

$$\text{electrons:} \qquad J_{nx} = q\mu_n \, n \, \mathcal{E}_x + qD_n \frac{dn}{dx} \tag{1.1}$$

$$\text{holes:} \qquad J_{px} = q\mu_p \, p \, \mathcal{E}_x + qD_p \frac{dp}{dx} \tag{1.2}$$

In Equations 1.1 and 1.2, q is the electronic charge, μ_n is the mobility of electrons, μ_p is the mobility of holes, n is the electron density, p is the hole density, $\mathcal{E}_x$ is the net electric field in the x direction, D_n is the diffusion constant for electrons and D_p is the diffusion constant for holes. If the semiconductor doping is non-uniform but of one type, there will be a built-in electric field that balances the diffusion tendency of free carriers with an opposing drift tendency. When a p-type and n-type semiconductor are brought into contact to form a pn junction, the dopant gradients are generally large and the depletion approximation is employed to describe carrier movement across the junction [1].

Current through a pn junction is the basis for BJT operation and is described by solutions to the continuity equation for free carriers. The continuity equation is basically an accounting for the flux of free carriers into and out of an infinitesimal volume inside a semiconductor. For a semiconductor in thermal equilibrium, the continuity equation includes the drift and diffusion mechanisms as well as the generation and recombination of carriers. The one-dimensional continuity equations for each carrier type is given by the following equations:

$$\frac{\partial n}{\partial t} = \mu_n n(x)\frac{\partial \mathcal{E}(x)}{\partial x} + \mu_n \mathcal{E}(x)\frac{\partial n(x)}{\partial x} + D_n \frac{\partial^2 n(x)}{\partial x^2} + (G_n - R_n) \tag{1.3}$$

$$\frac{\partial p}{\partial t} = \mu_p p(x)\frac{\partial \mathcal{E}(x)}{\partial x} + \mu_p \mathcal{E}(x)\frac{\partial p(x)}{\partial x} + D_p \frac{\partial^2 p(x)}{\partial x^2} + (G_p - R_p) \tag{1.4}$$

G_n, G_p and R_n, R_p represent the generation and recombination rates per unit volume for electrons and holes. Equations 1.3 and 1.4 assumes that the mobilities (μ_n, μ_p) and the diffusion constants (D_n, D_p) are not functions of x. By solving the continuity equation for minority carriers in the quasi-neutral[1] regions near a pn junction, the carrier densities can be obtained. This result combined with the boundary values for minority-carrier densities at the edges of the quasi-neutral regions make it possible

[1]Regions of the semiconductor where the net electric field is zero.

to obtain steady-state current-voltage characteristics of the *pn* junction. The IV characteristic of a single junction (or grouped junctions such as a BJT) determine the operational characteristics of the semiconductor device [1, 2, 3].

1.1.2 Carrier Generation and Recombination

The crystal-bonding model and the energy-band model of silicon help describe the direct transfer of carriers between the valence band and the conduction band in thermal equilibrium. In turn, these models describe a process of generation and recombination of electrons and holes that contribute to current in the semiconductor device. Due to the indirect band structure of silicon, carrier transitions between the valence band and the conduction band are not the dominant process for generation and recombination. In practice, localized states at energies between the valence band and the conduction band are always present because of lattice imperfections or defects. These defects can be caused by misplaced atoms in the crystal or, more usually, because of impurity atoms. Furthermore, defects are always present in sufficient numbers to dominate the generation-recombination process in silicon. Displacement damage due to radiation can also cause defects, which will be discussed in further detail in Section 1.3. The localized states act as stepping-stones for carriers to transition between the bands. For example, in a recombination event an electron falls from the conduction band to a localized state and then falls further into a vacant state in the valence band, thus recombining with a hole [1, 2, 3].

The four processes through which free carriers can interact with localized states are indicated in Figure 1.1. They are electron capture, electron emission, hole capture, and hole emission. The illustration shows a density (N_t) of states at an energy (E_t) within the forbidden gap. The states shown are acceptor type[2], but the processes

[2]Acceptor type states are neutral when unoccupied and negative when occupied.

described also apply to donor-type states [1].

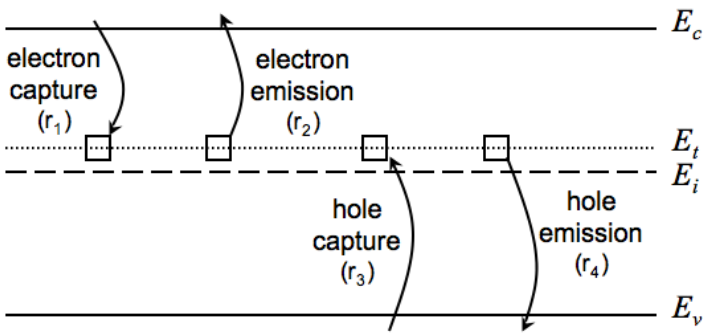

Figure 1.1: Interaction of free carriers with localized states.

In the first process, *electron capture*, an electron falls from the conduction band into an empty localized state. The rate at which this process occurs is proportional to the density of electrons n in the conduction band, the density of empty localized states, and the probability that an electron passes near a state and is captured by it. The density of empty localized states is given by their total density N_t times one minus the probability $f(E_t)$ that they are occupied. The probability per unit time that an electron is captured by a localized state is given by the product of the electron thermal velocity (v_{th}) and a parameter σ_n, called the *capture cross section*. The capture cross section describes the effectiveness of the localized state in capturing an electron. This product $v_{th}\sigma_n$ may be visualized as the volume swept out per unit time by a particle with cross section σ_n. If the localized state lies within this volume, the electron is captured by it. The capture cross section is generally determined experimentally for a given type of localized state. Combining all these factors, the total rate of capture of electron by the localized states is

$$r_1 = n\left\{N_t\left[1 - f(E_t)\right]\right\} v_{th}\sigma_n \tag{1.5}$$

The second process is *electron emission*, the inverse of electron capture. The emission of an electron from the localized state into the conduction band occurs at a rate given by the product of the density of states occupied by electrons $N_t f(E_t)$ times the probability e_n that the electron makes the jump (Equations 1.6 and 1.7). Equation 1.7 shows that electron emission from the localized state becomes more probable when its energy is closer to the conduction band.

$$r_2 = [N_t\, f(E_t)]\, e_n \tag{1.6}$$

$$e_n = v_{th}\sigma_n n_i \exp\left(\frac{E_t - E_i}{kT}\right) \tag{1.7}$$

Corresponding relationships describe the interactions between the localized states and the valence band. The third process, *hole capture*, describes the emission of an electron from the localized state to the valence band. It is proportional to the density of localized states occupied by electrons $N_t f(E_t)$, the density of holes and a transition probability. The transition probability is described by the product of the hole thermal velocity (v_{th}) and the capture cross section of a hole (σ_p) by the localized state. Thus the hole capture process is

$$r_3 = [N_t f(E_t)]\, p\, v_{th}\sigma_p \tag{1.8}$$

The fourth process, *hole emission*, describes the excitation of an electron from the valence band into the empty localized state. By arguments similar to those for electron emission, hole emission is given by

$$r_4 = \{N_t\,[1 - f(E_t)]\}\, e_p \tag{1.9}$$

$$e_p = v_{th}\sigma_p n_i \exp\left(\frac{E_i - E_t}{kT}\right) \tag{1.10}$$

Analogously to electron emission, the probability of emission of a hole from the localized state to the valence band becomes much greater as the energy of the state approaches the valence-band edge (Equation 1.10).

Qualitatively considering the physics of these four processes shows that at thermal equilibrium $r_1 = r_2$ and $r_3 = r_4$ since thermal equilibrium requires every process to be balanced by its inverse. In a non-equilibrium situation, $r_1 \neq r_2$ and $r_3 \neq r_4$. To gain insight about these rates, imagine specifically that holes in an n-type semiconductor are suddenly increased in number above their thermal equilibrium value. This would cause the hole capture process (r_3) to increase. The effect of this rate increase would increase hole emission (r_4) and electron capture (r_1), both of which eliminate holes at E_t. If most of the holes disappear from E_t via r_1, they will remove electrons from the conduction band, and the localized state will be an effective *recombination center*. If the holes are removed from the level at E_t predominantly by an increase in r_4, they will return to the valence band, and the site will be effective as a *hole trap*. A given localized state will generally be effective in only one way: either as a trap or as a recombination center.

Shockley-Read-Hall Theory of Recombination

The equations describing generation and recombination through recombination centers were originally derived by W. Shockley, W. T. Read and by R. N. Hall [4, 5]. The process is frequently referred to as Shockley-Read-Hall (SRH) recombination. According to the SRH model, when non-equilibrium occurs in a semiconductor, the overall population of the recombination centers is not greatly affected. There are so many majority carriers present that the recombination centers quickly capture them but have to wait for the arrival of a minority carrier. Thus, the states are nearly always full of majority carriers in either thermal equilibrium or non-equilibrium conditions. The net rate of recombination is a function of the density of free carriers, the

energy level of the recombination center, and the rate that carriers are captured as described in the following equation for an n-type semiconductor with acceptor-like recombination centers:

$$U \equiv R_{sp} - G_{sp} = \frac{N_t \, v_{th} \, \sigma_n \, \sigma_p \, (pn - n_i^2)}{\sigma_p \left[p + n_i \exp\left(\frac{E_i - E_t}{kT}\right)\right] + \sigma_n \left[n + n_i \exp\left(\frac{E_t - E_i}{kT}\right)\right]} \tag{1.11}$$

The subscript *sp* stands for *spontaneous*, meaning that it describes the recombination and generation that responds only to deviation from thermal equilibrium. The term $(pn - n_i^2)$ represents the restoring force for free-carrier populations in a non-equilibrium condition. There is a net recombination if the pn product exceeds n_i^2 and there is a net generation if the pn product is less than n_i^2.

The dependence of U on the energy level of the recombination center can be more easily grasped if the electron and hole capture cross sections are considered to be equal. For the case $\sigma_p = \sigma_n \equiv \sigma_o$, then $\tau_o \equiv (N_t v_{th} \sigma_o)^{-1}$ can be defined and the net recombination rate is

$$U = \frac{(pn - n_i^2)}{\left[p + n + 2n_i \cosh\left(\frac{E_t - E_i}{kT}\right)\right] \tau_o} \tag{1.12}$$

The hyperbolic cosine term of Equation 1.12 shows that the recombination rate is dependent on the energy level of the recombination center. This term is symmetric around $E_t = E_i$, which reflects a symmetry in the capture of holes and electrons by the center. The denominator is at its minimum value when $E_t = E_i$, so that U is maximized for recombination centers having energies near the middle of the band gap. The major results of the SRH recombination analysis show that the net recombination rate will be a function of free-carrier densities as well as the energy level of recombination center.

Excess-Carrier Lifetime

To understand the physical significance of the net recombination rate U, consider a semiconductor with no current flow (i.e. no drift and diffusion mechanisms) in which thermal equilibrium is disturbed by the sudden creation of equal numbers of excess electrons and holes. These excess carriers then decay spontaneously as the semiconductor returns to thermal equilibrium. Solutions of the continuity equations for this case give the excess electron density as a function of time. Assuming that the disturbance of equilibrium corresponds to low-level injection,[3] then the external disturbance does not appreciably change the total free-carrier density from its equilibrium value. If n' is the extra injected electron density and p' is the extra hole density, then low-level injection implies that n' and p' are both much less then $(n_o + p_o)$ where n_o and p_o represent the thermal-equilibrium densities of carriers in the semiconductor. From these definitions, $n' \equiv n - n_o$ and $p' \equiv p - p_o$, where $n' = p'$.

If $\sigma_n = \sigma_p$, then the recombination rate is given by Equation 1.12 and the continuity equation can be written

$$\frac{dn'}{dt} = -U = \frac{-\left(n_o + p_o\right) n'}{\left(n_o + p_o + 2n_i \cosh\left[\frac{E_t - E_i}{kT}\right]\right) \tau_o} \tag{1.13}$$

Solving for n', then the excess carrier density decays exponentially with time

$$n'(t) = n'(0) \exp(-t/\tau_n) \tag{1.14}$$

where the *lifetime* τ_n is given by

$$\tau_n = \left[\frac{n_o + p_o + 2n_i \cosh\left(\frac{E_t - E_i}{kT}\right)}{\left(n_o + p_o\right)}\right] \tau_o \tag{1.15}$$

[3]Low-level injection means that the excess carrier concentration is much less than the thermal equilibrium majority carrier concentration.

As noted in the previous section, the most effective recombination centers will have E_t close to E_i. Therefore, the net recombination rate is reduced to

$$U = \frac{n'}{\tau_n} \tag{1.16}$$

$$\tau_n = \tau_o = \frac{1}{N_t v_{th} \sigma_o} \tag{1.17}$$

Equation 1.17 shows that the excess carrier lifetime is independent of the majority carrier concentration for recombination through recombination centers under low-level injection. For example, in a p-type semiconductor most of the recombination centers are empty of electrons since the Fermi energy level is less than the trap energy level (assuming traps near midgap). The recombination process is therefore limited by the capture of electrons from the conduction band. Once an electron is captured by a recombination center, one of the many holes in the valence band is quickly captured. Thus, the rate-limiting step in the recombination process is the capture of a minority carrier by the recombination center [1].

1.1.3 IV Characteristics of *pn* Junctions

Solutions to the continuity equations of uniformly doped step-junctions together with the concept of excess-carrier lifetime as derived from the SRH recombination model allow an equation to be derived for current in a pn junction under bias. The equation, generally know as the ideal-diode equation shows that the current is dependent on voltage [1, 2]. The ideal-diode equation, in terms of current density, is:

$$J_t = J_o \left(e^{\left(\frac{qV_a}{kT}\right)} - 1 \right) \tag{1.18}$$

where: J_o = reverse saturation current density

V_a = applied voltage

Equation 1.18 infers that current in a *pn* junction will rapidly increase with an applied positive voltage. An applied positive voltage, or forward bias, is such that the *p*-region is positive with respect to the *n*-region. In this situation, holes are injected from the *p*-region and electrons are injected from the *n*-region. These are majority carriers in each region, and their supply is plentiful near the junction. Equation 1.18 also infers that current is much smaller under reverse bias. Under this condition, current is due to minority carriers that are generated either in the junction depletion region or nearby.

Depletion Region Currents

The analysis of *pn* junctions that led to the ideal-diode equation was based on conditions in the quasi-neutral regions. The depletion region was treated solely as a barrier of the diffusion of majority carriers, and it played a role only in the establishment of minority-carrier densities at its boundaries. In practical diodes, currents that result from phenomena in the depletion region must be considered.

The depletion region typically has dimensions on the order of 10^{-4}cm. Like the quasi-neutral zones of the *pn* junction, it contains generation-recombination centers; unlike the quasi-neutral zones, it is a region of steep impurity gradients and rapidly changing populations of holes and electrons. Since the injected carriers, under forward bias, must pass through this region, some carriers may be lost by recombination. Using the SRH theory of recombination and assuming equal hole and electron capture cross sections, the recombination rate in the depletion region with an applied bias V_a is:

$$U = \frac{n_i^2 \left(e^{\left(\frac{qV_a}{kT}\right)} - 1 \right)}{\left(p + n + 2n_i \cosh\left(\frac{E_t - E_i}{kT}\right) \right) \tau_o} \tag{1.19}$$

The recombination rate is thus positive for forward bias and negative under reverse bias. The total current arising from generation and recombination in the depletion region is given by the integral of the recombination rate across it:

$$J_r = q \int_{-x_p}^{x_n} U \cdot dx \tag{1.20}$$

The recombination current is found by evaluating the integral for a maximum value of U extending across a portion[4] (x') of the depletion region. Recombination centers are most effective when they are located near the middle of the bandgap. Also, from Equation 1.19, it is evident that U is maximized when the sum $p + n$ is minimized. Therefore, for the conditions, $E_t = E_i$ and $p = n = n_i \exp\left(\frac{qV_a}{2kT}\right)$, the recombination current is

$$J_r = \frac{qx' n_i^2 \left(e^{\left(\frac{qV_a}{kT}\right)} - 1\right)}{2n_i \left(e^{\left(\frac{qV_a}{2kT}\right)} + 1\right) \tau_o}$$

$$J_r \approx \frac{qx' n_i}{2\tau_o} \exp\left(\frac{qV_a}{2kT}\right) \tag{1.21}$$

Under low forward bias, this current dominates over the ideal-diode current. Therefore, current that results from recombination in the depletion region must be added to the ideal-diode equation to obtain the overall current-voltage relationship.

Similarly, under reverse bias, there is a net generation current in the depletion region that dominates over the ideal-diode current. However, reverse-biased junction current is still much smaller than forward-biased junction. The net generation current can be approximated by the product of the maximum generation rate and a width (x_i) of the depletion region [1]:

$$J_g = \frac{qn_i x_i}{2\tau_o} \tag{1.22}$$

[4] x' is often approximated by the entire depletion region width.

$$x_i = \left(\frac{2\epsilon_s kT}{q^2 N_d}\right)^2 \left[\left(\ln\frac{N_d}{n_i} - \frac{qV_a}{kT}\right)^{1/2} - \left(\ln\frac{N_d}{n_i}\right)^{1/2}\right] \tag{1.23}$$

Because the density of recombination centers in practical diodes may vary with position and is generally not well known, it is often not worthwhile to distinguish between x_i and the entire depletion region (x_d). This is also true for x' in Equation 1.21.

Analysis of currents in the depletion region indicates that generation and recombination of carriers leads to added current components. The observed steady-state dependence of current on voltage for a *pn* junction is made up of the superposition of the ideal-diode current and these components. This result is important for understanding the operation of a BJT.

1.2 The Bipolar Junction Transistor

The bipolar junction transistor is a multi-junction semiconductor device that, in conjunction with other circuit elements, is capable of current gain, voltage gain, and signal-power gain [1, 2, 3]. In its simplest form a BJT is a three-region device with two diodes arranged back-to-back and the base region is common to both (Figure 1.2). Locating two junctions in close proximity allows the modulation of the current in one *pn* junction by changing the bias on the nearby junction. Fundamental BJT operation, therefore, can be construed as the physical and electrical behavior of majority and minority carriers, the latter from their injection into the base at the emitter-base junction, their transport through the base en route to the collector, and their retrieval, as majority carriers, by the collector, across the base-collector junction. The voltage across the base-emitter junction controls the number of carriers per second injected into the base region. To a first approximation, the device looks like a voltage-controlled current source where the current in the collector is controlled by the base-emitter voltage.

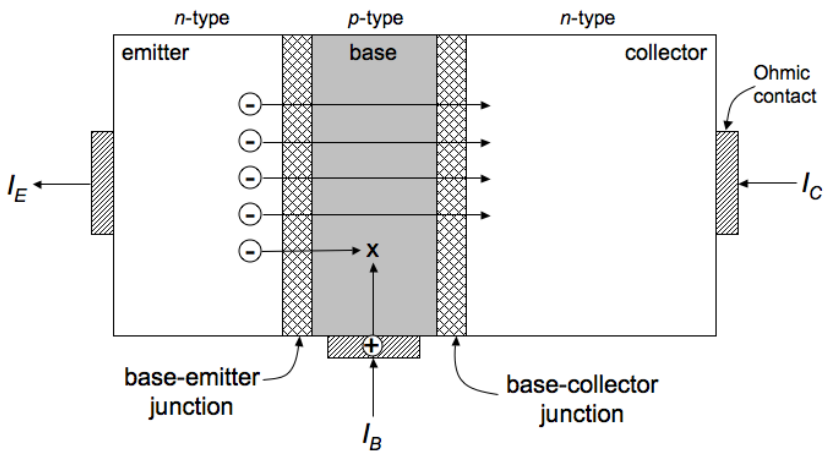

Figure 1.2: A simplified depiction of BJT operation.

There are four operating modes of a BJT determined by the bias of the device. Figure 1.3 defines the regions of device operation in terms of the applied junction voltages. Switching applications design a BJT to operate in the saturated and cut-off

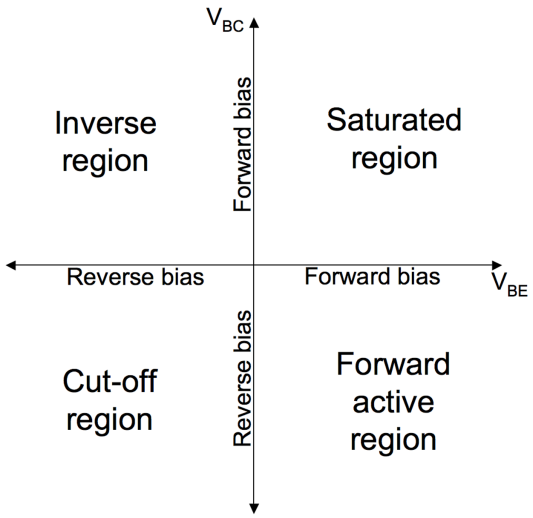

Figure 1.3: Regions of operation for a BJT.

regions. However, a MOSFET is generally used to perform this type of application in integrated circuits because its characteristics allow more efficient switching action.

On the other hand, BJTs usually have a higher transconductance than MOSFETs. To take advantage of the high transconductance, most analog applications design a BJT to be exercised as an amplifier, which corresponds to operating it in the forward-active region of operation. Consequently, this work concentrates on the operation of a *npn* BJT in the forward-active region. For a *npn* transistor, the forward-active bias condition results in electron injection at the emitter-base junction and electron collection at the base-collector junction.

A simple and useful model of the carrier injection and extraction phenomena occurring in BJTs was developed by J. J. Ebers and J. L. Moll [6]. The Ebers-Moll model is based upon the interacting diode junctions and is valid for all regions of operation. The Ebers-Moll equations express the solutions to the two diode equations formally and ultimately describe the current in each terminal of the BJT. The reference currents, I_{CC} and I_{EC}, represent those currents that are collected or transported across the base. The reference collector source current (I_{CC}) and the reference emitter source current (I_{EC}) can be written as:

$$I_{CC} = I_S \left(e^{\frac{qV_{BE}}{kT}} - 1 \right) \tag{1.24}$$

$$I_{EC} = I_S \left(e^{\frac{qV_{BC}}{kT}} - 1 \right) \tag{1.25}$$

where I_S is the transistor saturation current, V_{BE} is the voltage across the base-emitter junction and V_{BC} is the voltage across the base-collector junction. These two reference currents can express the BJT's terminal currents as:

$$I_B = \left(\frac{1}{\alpha_F} - 1 \right) I_{CC} + \left(\frac{1}{\alpha_R} - 1 \right) I_{EC} \tag{1.26}$$

$$I_C = I_{CC} - \frac{I_{EC}}{\alpha_R} \tag{1.27}$$

$$I_E = -\frac{I_{CC}}{\alpha_F} + I_{EC} \tag{1.28}$$

The constants α_F and α_R are related to the large-signal forward and reverse DC current gains of a common-emitter transistor (β_F and β_R, respectively) by the expressions:

$$\beta_F = \frac{\alpha_F}{1-\alpha_F} \tag{1.29}$$

$$\beta_R = \frac{\alpha_R}{1-\alpha_R} \tag{1.30}$$

Analysis of bipolar transistor performance in a circuit is best accomplished with mathematical models, such as the Ebers-Moll model. Although the Ebers-Moll model provides simple, non-linear relationships between the terminal currents and voltages, it neglects important second-order effects seen in actual BJTs. The charge-control model of the BJT developed by H. K. Gummel and H. C. Poon addresses some of these effects [7]. As a result, it has been an industry-standard BJT model for circuit simulators since its inception. Details about characterizing a bipolar transistor using the Gummel-Poon model are discussed in Chapter 3.

The common-emitter DC current gain (β) is an important characteristic for a BJT. It is defined as the ratio of the collector current to the base current ($\beta = \frac{I_C}{I_B}$), so it provides a critical performance metric for operation in a circuit. Since the crucial part of BJT action occurs in the base region, the mechanisms that contribute to the base current must be understood. Under low-level injection there are five components that contribute to the base current of a *npn* transistor biased in the foward-active region as shown in Figure 1.4. The reverse diffusion current (I'_D) is due to injection of holes from the base into the emitter. The recombination-generation current (I_{RG}) and the surface current (I_S) are produced by majority carriers flowing into the base-emitter space-charge region, whereas the collector leakage current (I_{CBO}) is produced primarily by carriers flowing out of the base-collector space-charge region. As a result I_{CBO} is in the direction opposite to the other four base current components. The base

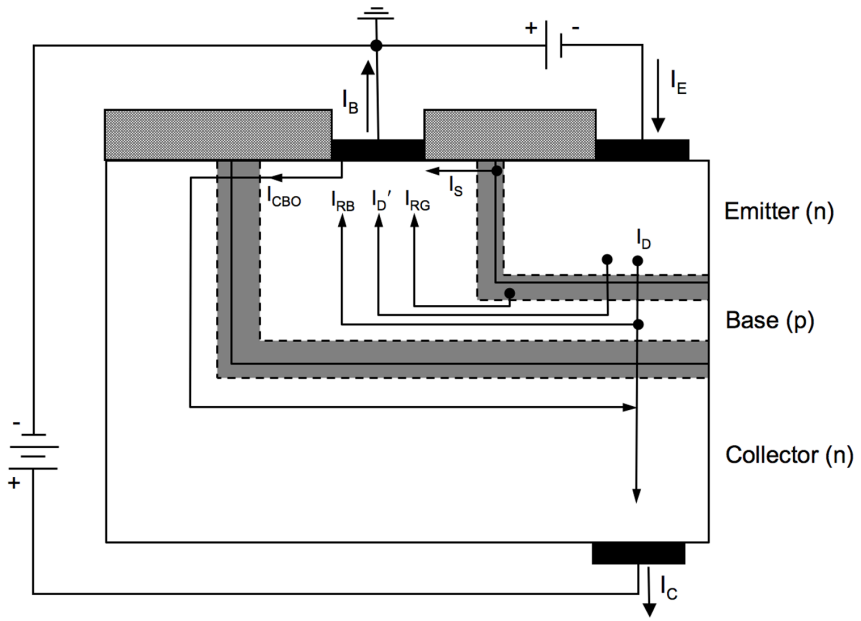

Figure 1.4: Schematic representation of base current components.

recombination current (I_{RB}) is due to the recombination of excess minority carrier electrons with majority carrier holes in the base. Using the base current components the common-emitter DC current gain is:

$$\beta = \frac{I_C}{I_B} = \frac{I_C}{I'_D + I_{RG} + I_S + I_{RB} - I_{CB0}} \tag{1.31}$$

Fundamental operation of a BJT is dependent on minority carriers in the base region. Consequently, the common emitter current gain degrades when minority carriers are eliminated in the base region, as described in a recombination event. Therefore, the base current components due to recombination (I_{RB}, I_{RG}, I_S) are important factors in developing the neutron-effects BJT model. The damage effects of neutrons on the electrical behavior of semiconductor devices, specifically BJTs, are discussed in further detail in Section 1.3.

1.3 Neutron Damage Effects in Silicon

Radiation affects semiconductors through two fundamental damage mechanisms: lattice displacement and ionization [8, 9, 10]. Lattice displacement refers to the physical damage to a crystal lattice produced by knocking an atom from its normal position to another location in the lattice. Ionization is the knocking of orbital electrons from an atom to form ionized atoms and free electrons. Neutron radiation is the dominant source of lattice displacement in semiconductor material and is the effect focused on for this work.

When high-energy neutrons collide with the semiconductor lattice, atoms become dislodged from their lattice site to interstitial positions within the crystal. The former site of the now displaced atom in the lattice is called a vacancy. The displaced atom is called an interstitial, and the interstitial-vacancy pair is called a Frenkel pair. If the energy of the incident neutron is sufficiently large, it can impart enough energy to the displaced atom for it, in turn, to displace other atoms in the lattice (Figure 1.5). As a result, the damage caused by neutron irradiation usually involves a large disordered region called a defect cluster.

Once defects are formed by incident fast neutrons, they reorder in a number of possible combinations. Eventually, all displaced atoms lose sufficient energy to achieve thermal equilibrium within the lattice. Some of the atoms slip back into the vacancy to reconstitute the local lattice structure. Other atoms combine with dopant atoms to produce stable defects. Vacancies in silicon are quite mobile at room temperatue. Mobile vacancies can combine with the impurity atoms, donor atoms, or other vacancies to produce room temperature stable defects.

Although defect reordering produces more stable configurations, any disturbance of lattice periodicity may produce energy levels in the bandgap. Relevant literature on the subject has reported that radiation-induced levels in the bandgap can give rise

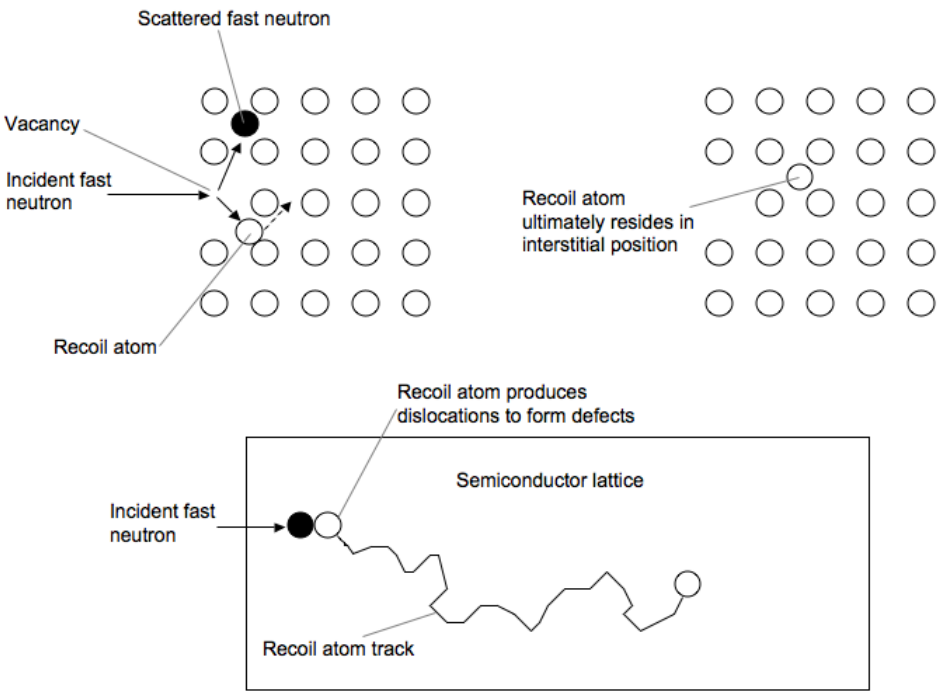

Figure 1.5: Production of defects by fast neutrons.

to several processes, including generation, recombination, trapping, compensation, tunneling, scattering, type conversion, and field enhancement of carrier generation effectiveness [8]. These processes have a major impact on the electrical behavior of semiconductor devices. Specifically for BJTs, the common emitter current gain is significantly degraded. Studies on the effects of displacement damage on BJTs indicate that the dominant mechanism for gain degradation is due to the introduction of recombination centers throughout the device [11]-[17]. This leads to an increase in carrier recombination rate, reducing the lifetime of minority carriers. As discussed previously, the fundamental operation of a BJT is dependent on minority carriers in the base region.

1.4 Research Focus

The purpose of this research is to gain a better physical understanding of the damage effects of neutrons on semiconductor devices, in particular BJTs, and develop a compact model for IC analysis and design. Historical studies on displacement damage effects on semiconductor devices is applied in the development of the model. The work emphasizes model development for the large-signal, static DC characteristics of a BJT test structure operating in the forward-active mode. The BJT test structure was fabricated in a bulk silicon, radiation-hardened, $0.6\,\mu m$ CMOS technology. Current-voltage relationships that describe the neutron damage effects are developed and applied to the existing Gummel-Poon BJT model. Two separate approaches were taken to describe the damage effects. Both methods add a current component to the BJT's base current. The first method is based on a non-ideal diode equation while the second method is based on the SRH theory of recombination.

Chapter 2

Device Characterization

This chapter overviews the fabrication technology used for the bipolar transistor devices of interest, as well as the testing conditions and procedures. The BJTs are test structures for the process technology. The testing procedures for the devices were conducted as part of a qualification of an Application-Specific Integrated Circuit (ASIC) for use in a radiation environment. It is from these data that the device model with neutron damage effects was developed. Since the device model was calibrated to experimental data, key device parameters of the model are determined by the process and performance of the devices. Therefore, it is important to survey the technology that the devices were made in as well as characterize the performance of the several devices at various environmental conditions that affect their operation.

2.1 Process Technology

The bipolar junction transistor was fabricated at the Microelectronics Development Laboratory, located at Sandia National Laboratories in Albuquerque, NM. The fabrication process, CMOS6RA, is a bulk silicon, radiation-hardened, 0.6 μm minimum feature size, 5 V CMOS technology. This process employs special proprietary techniques to reduce the sensitivity of devices, especially MOSFETs, to radiation effects such as total-ionizing-dose and single-event effects. Therefore, the process will not be discussed in detail.

The BJT under investigation is a vertical *npn* structure. The simplified cross section of the device, shown in Figure 2.1, provides basic geometries and doping levels of the device. The structure is a standard *npn* bipolar device for the technology. Fabrication of a BJT in a CMOS process aides designers in optimizing certain analog circuits, as was the case for this device. However, the performance, i.e. current gain, of the BJT is usually less than it would be in a bipolar technology.

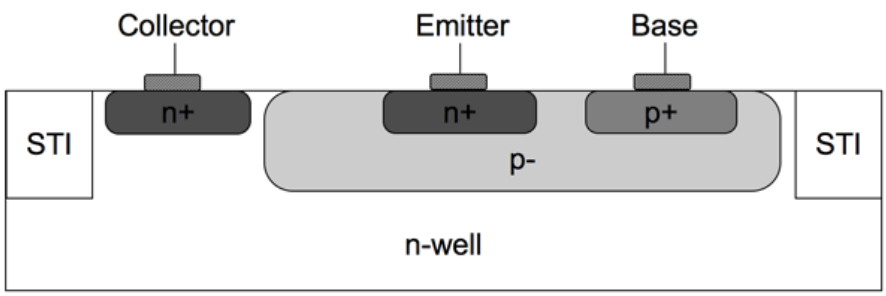

Figure 2.1: Cross section of CMOS6RA vertical *npn* bipolar transistor.

2.2 Device Testing and Analysis

The bipolar transistors were subjected to experiments required to qualify an ASIC for use in a radiation environment. There are two components of concern in determining the experimental setup: radiation exposure and device performance characterization. The tests for these devices were performed at the wafer level.

2.2.1 Radiation Exposure

The devices were exposed to neutron radiation at the Annular Core Research Reactor (ACRR), which is a pool type research reactor with a large, irradiation cavity in the core center. For the experiment, a wafer was divided in 4 sections and each quarter was exposed to neutron radiation at specified fluence levels. Fluence (Φ) is the total number of particles penetrating a given area cross section (cm^2) from all directions, and all energies [10]. The reactor produces an energy spectrum of neutrons and the fluence levels are referenced to 1 MeV equivalent silicon damage. The devices were at room temperature and unbiased during radiation exposure. Table 2.1 indicates the fluence levels for each quarter of the wafer.

Table 2.1: BJT neutron radiation exposure by fluence level.

Wafer Quarter	Fluence (neutrons/cm^2)
1	1×10^{12}
2	1×10^{13}
3	1×10^{14}
4	3×10^{13}

2.2.2 Device Performance Characterization

Several tests were conducted to analyze the performance of the bipolar transistors before and after neutron irradiation. The experimental data used to develop the device model were based on the forward-Gummel test. A schematic of the test is shown in Figure 2.2. In this schematic, the collector is connected to SMU3 and held at a constant voltage of 2.0 V, the base is connected to SMU2 and held at a constant voltage of 0 V, and the emitter, connected to SMU1, is swept from 0 V to −1.0 V in −0.05 V increments.

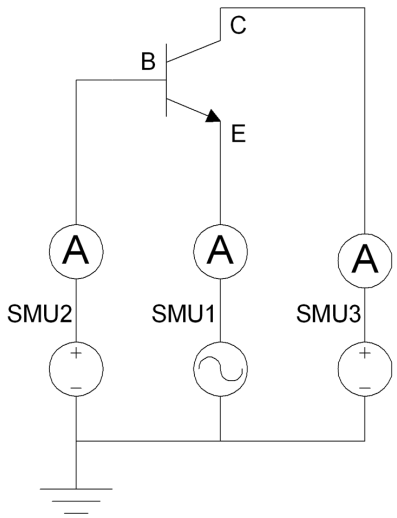

Figure 2.2: Test set up for forward Gummel device characterization.

The forward-Gummel test characterizes the current-voltage relationship of the device in the forward-active region by measuring the collector, base, and emitter currents, from which the current gain (β) is calculated. All devices on two wafers were characterized before and after irradiation. One wafer was exercised as a control factor and did not receive radiation exposure. The second wafer was exposed to neutron radiation as described previously. All measurements were conducted at room

temperature and the BJTs did not experience any type of thermal cycling before, during, or after radiation exposure. In addition, the measurements after radiation were taken several months following exposure. The environmental conditions before, during and after radiation were intended to allow the characterization of long-term-annealed BJTs.

Figure 2.3 shows typical forward-Gummel plots for the *npn* devices before and after neutron irradiation. The plot on the left is the base current, and the plot on the right is the collector current. Both I_B and I_C are plotted as a function of the base-emitter voltage (V_{BE}). This transistor was exposed to a radiation level of 1×10^{14} neutrons/cm^2.

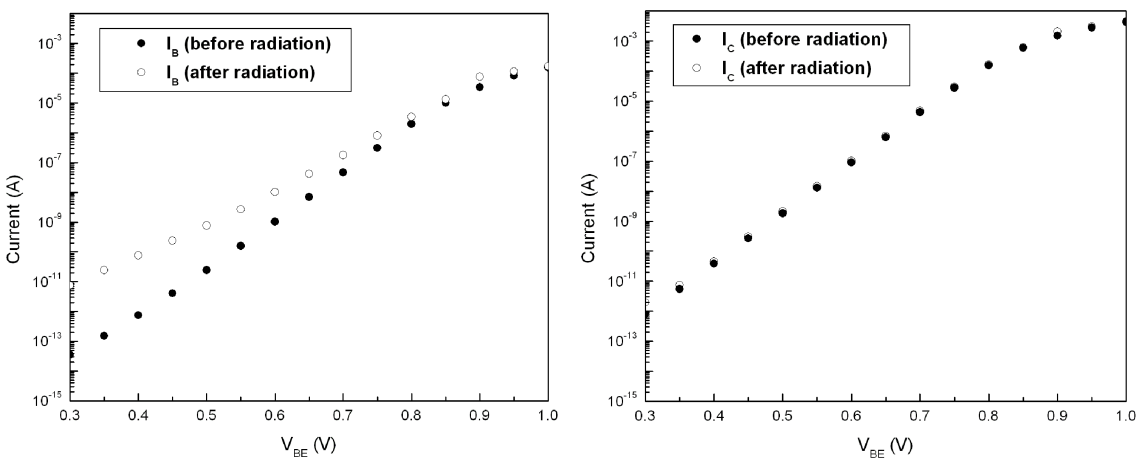

Figure 2.3: Typical Gummel plots of the base current (I_B) and the collector current (I_C) as a function of the base-emitter voltage (V_{BE}) before and after irradiation.

The effect of neutron damage is most pronounced in the base current, so the data are in agreement with previous studies of displacement damage effects on BJTs [8]-[18]. Since the dominant mechanism for degradation of the BJT common-emitter current gain is due to the introduction of recombination centers, the gain of a BJT

operating in the forward-active region can be expressed as [9]:

$$\beta(\text{after radiation}) = \frac{I_C}{I_{B0} + \Delta I_B} \tag{2.1}$$

Current gain is inversely proportional to the base current and Equation 2.1 implies that additional base current components due to recombination (ΔI_B) can account for the gain degradation. This result is important in developing a compact model of the effects of neutron damage on bipolar transistors.

Chapter 3

Compact BJT Modeling

The term 'compact model' refers to the lumped models used by circuit simulators. More specifically, it generally refers to the mathematical models of semiconductor components commonly incorporated into SPICE[1]. Although of paramount importance to IC design, these models are difficult to enhance because they are largely implemented in C code that is compiled into the simulator. As a result, neutron-effects modeling of BJTs at the circuit level has been done by manipulating existing model parameters as a function of fluence [19, 20, 21].

The approach taken in the development of a compact model for Sandia's BJT test structure was to add physics-based neutron effects directly to the model. The hardware description language (HDL) Verilog-A allowed for this approach by providing the standard Gummel-Poon BJT model in source form. Furthermore, Verilog-A is a standard language that SPICE-type circuit simulators understand, so the models are portable [22]. This chapter describes the development of the compact BJT model with neutron damage effects beginning with a description of the Gummel-Poon BJT model as implemented in Verilog-A.

[1]SPICE is an acronym for Simulation Program with IC Emphasis.

3.1 Gummel-Poon BJT Model

The BJT model developed by H. K. Gummel and H. C. Poon [7] was implemented in the industry-standard circuit simulation tool SPICE in the early 1970's and is still in use today. It provides designers a computationally fast, physics-based model of BJT behavior in a circuit under various bias conditions. A circuit representation of the Gummel-Poon BJT model [23] is shown in Figure 3.1. The diodes between the base and emitter represent current through the junction from ideal components and non-ideal components. The non-ideal components of the base current are caused by the recombination of carriers at the surface, recombination of carriers in the base-emitter depletion region, and the formation of base-emitter surface channels. Similarly, ideal and non-ideal components of the collector current are also represented by diodes between the base and collector. The Gummel-Poon model includes the effects of low current drop in transistor current gain, base-width modulation, high-level injection, and the current dependence of the base resistance. The model describes the intrinsic part of the transistor in three basic equations that express base current, collector current, and total stored charge in the base as a function of voltage bias [24, 25].

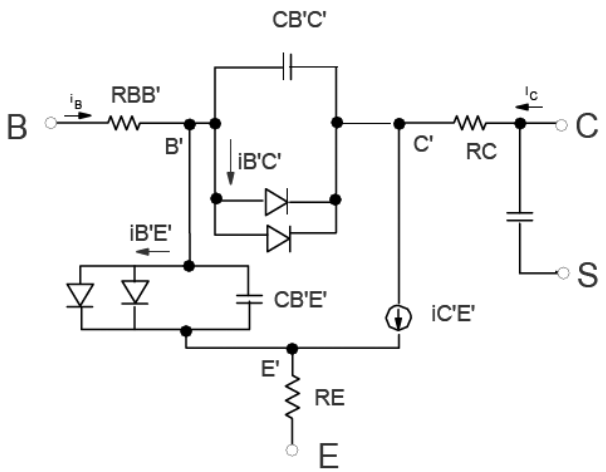

Figure 3.1: Gummel-Poon large signal circuit schematic of a BJT.

G-P Model Implementation in Verilog-A

The Gummel-Poon BJT model written in Verilog-A HDL is compatible with most commercial SPICE-based simulators. The following model equations define the DC characteristics of a BJT operating in the forward active region: (A conductance GMIN term is added to the equations to aid in convergence.)

$$\begin{aligned} I_B &= I_S\left[\frac{1}{\beta_F}\left(e^{\frac{qV_{BE}}{n_F kT}}-1\right)-\frac{1}{\beta_R}\right]+I_{SE}\left(e^{\frac{qV_{BE}}{n_E kT}}-1\right)- \\ &\quad I_{SC}+\left(\frac{V_{BE}}{\beta_F}+\frac{V_{BC}}{\beta_R}\right)\text{GMIN} \end{aligned} \tag{3.1}$$

$$\begin{aligned} I_C &= \frac{I_S}{q_b}\left(e^{\frac{qV_{BE}}{n_F kT}}+\frac{q_b}{\beta_R}\right)+I_{SC}+ \\ &\quad \left[\frac{V_{BE}}{q_b}-\left(\frac{1}{q_b}+\frac{1}{\beta_R}\right)V_{BC}\right]\text{GMIN} \end{aligned} \tag{3.2}$$

$$q_b = \frac{q_1}{2}\left[1+\sqrt{1+4q_2}\right] \tag{3.3}$$

where

$$q_1 = \left(1-\frac{V_{BC}}{V_{AF}}-\frac{V_{BE}}{V_{AR}}\right)^{-1}$$

$$q_2 = \frac{I_S}{I_{KF}}\left(e^{\frac{qV_{BE}}{n_F kT}}-1\right)-\frac{I_S}{I_{KR}}+\left(\frac{V_{BE}}{I_{KF}}+\frac{V_{BC}}{I_{KR}}\right)\text{GMIN}$$

Gummel-Poon model parameter extraction

The complete specification of a BJT model requires fundamental physical constants, operating conditions, and model parameters [24, 25]. Physical constants, such as Boltzmann's constant (k) and electronic charge (q) are normally defined in program code. The operating conditions define the circumstances under which the model

equations are to be used. Model parameters describe the device for a given set of operating conditions and are unique to each device in a circuit. The values of model parameters can be extracted from measurement data and must be supplied to the model by the user. Accurate circuit simulation requires accurate and meaningful parameter values for each model. The measurement techniques to extract forward-biased DC parameters for the Gummel-Poon model utilized IC-CAP[2] Parameter Extraction and Device Modeling software and an HP4155 Semiconductor Parameter Analyzer. The electrical behavior represented by the static Gummel-Poon model is depicted in $\ln I_C$, $\ln I_B$ vs. V_{BE} curves. This measurement data for the *npn* devices before exposure to radiation were averaged to determine baseline parameter values. Table 3.1 displays the physical meaning and extracted values of the parameters required for the Gummel-Poon BJT model in the forward-active operating region. Extraction of these parameters enabled simulation of the BJT in Silvaco's SmartSPICE program that closely matched the measured data. Thus, a BJT model was defined, which served as a basis for neutron model development.

Table 3.1: Gummel-Poon Model Parameters for a BJT in the Forward-Active Region.

Parameter	Description	Value
I_S	Saturation current	7.596×10^{-18} A
I_{SE}	Non-ideal base-emitter saturation current	3.843×10^{-17} A
I_{SC}	Non-ideal base-collector saturation current	0.0 A
β_F	Ideal maximum forward current gain	91.61
β_R	Ideal maximum reverse current gain	1
n_F	Forward current emission coefficient	0.9985
n_E	Base-emitter leakage emission coefficient	1.599
V_{AF}	Forward early voltage	1000 V
V_{AR}	Reverse early voltage	1000 V
I_{KF}	Corner for forward β high-current roll-off	1.654×10^{-03} A
I_{KR}	Corner for reverse β high-current roll-off	10 A

[2]IC-CAP is an acronym for Integrated Circuit Characterization and Analysis Program.

3.2 Compact Modeling of Neutron Damage

Many studies of displacement damage mechanisms in BJTs have indicated that the common-emitter current gain degrades through the introduction of recombination centers[8]-[18]. In addition, measurement data of BJTs before and after radiation indicate that the effect of neutron damage is most pronounced on the base current of the BJT. To incorporate the static effects of neutron radiation damage in the Gummel-Poon model, an equation describing the introduction of recombination centers was added to the base current equation. The end result provides a BJT neutron model that describes the behavior of a fully-annealed device.

3.2.1 BJT Model with Neutron Damage Effects: Non-ideal Diode Equation

The Gummel-Poon model provides a more accurate representation of BJTs over the Ebers-Moll model because it includes the effects at low-current, high-level injection, and a complete description of base-width modulation[3]. The effects at low-current result from additional base current due to recombination that degrades the current gain. The mechanism for current gain degradation from neutron radiation damage is also due to recombination. Therefore, one approach to incorporate static neutron damage effects is to add a term to the base current equation similar to the the Gummel-Poon term that describes low-current effects.

Recombination Currents

As described in Section 1.1.3, recombination in the depletion region leads to a modified diode relationship for the junction currents at low forward-bias conditions. It

[3]For a complete description the Gummel-Poon model, see [7, 24, 25].

is evident from Figure 3.2 that BJT current gain degradation at low currents (Region I) presents itself in the base current [24]. The extra components of I_B are

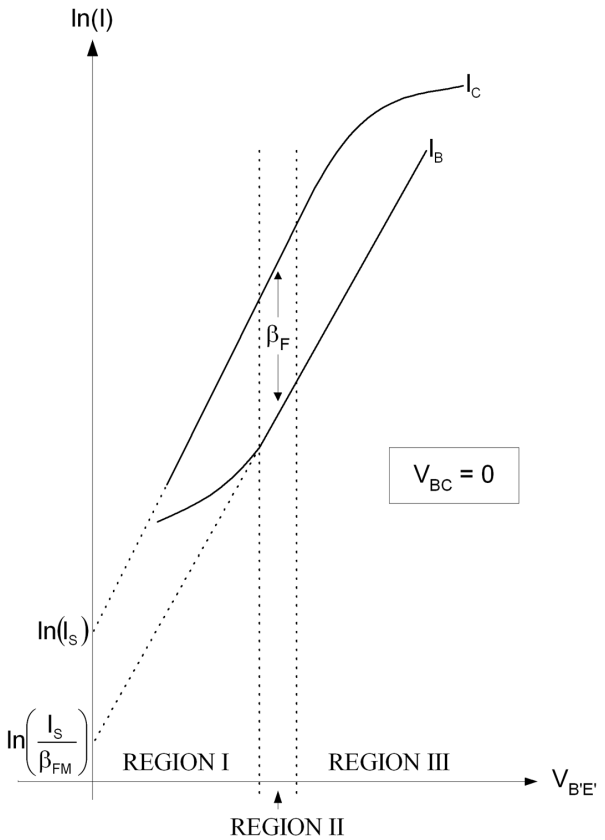

Figure 3.2: Graph of $\ln I_C$ and $\ln I_B$ as a function of V_{BE}. Region I is the low-current region, Region II is the mid-current region, and Region III is the high-current region.

caused by (1) the recombination of carriers at the surface, (2) the recombination of carriers in the emitter-base depletion region and, (3) the formation of emitter-base surface channels. Channeling and surface recombination can both be made small with careful processing, so the dominant component is normally the recombination in the emitter-base depletion region. The recombination rate in the depletion region was given by

$$U = \frac{n_i^2 \left(e^{\left(\frac{qV_a}{kT}\right)} - 1\right)}{\left(p + n + 2n_i \cosh\left(\frac{E_t - E_i}{kT}\right)\right) \tau_o} \tag{3.4}$$

Since the depletion region is mostly depleted of carriers, then this area can be considered intrinsic. In other words, the density of electrons and holes are roughly equal to each other so the Fermi level, denoted E_i, is in the middle of the forbidden gap. The most effective recombination centers also have an energy near the middle of the forbidden gap. Thus, $E_t = E_i$ and Equation 3.4 becomes

$$U = \frac{n_i^2 \left(e^{\left(\frac{qV_a}{kT}\right)} - 1 \right)}{(p + n + 2n_i)\,\tau_o} \tag{3.5}$$

It is deduced from Equation 3.5 that the recombination rate is maximized when the sum $p + n$ is minimized. For a semiconductor under non-equilibrium conditions the np product is a function of the applied bias and in the emitter-base depletion region of a BJT is given by

$$np = n_i^2 e^{\frac{qVBE}{kT}} \tag{3.6}$$

If the sum $p+n$ is considered as a variable function in p and n that is subject to the np product, then U is maximized when $p = n = n_i e^{\frac{qV_{BE}}{2kT}}$. The total current is given by the integral of the recombination rate across the depletion region

$$J_r = q \int_{-x_p}^{x_n} U \cdot dx \tag{3.7}$$

Therefore, the recombination current is maximized when the density of electrons and holes are equal as they are in the depletion region of the emitter-base junction. This result is also evident in a TCAD (Davinci) simulation of a carrier recombination with bulk traps in the base-emitter junction (Figure 3.3) [26]. For the simulation, the green region is the emitter (n-type Si), the yellow region is the base (p-type Si), and the blue region is oxide.

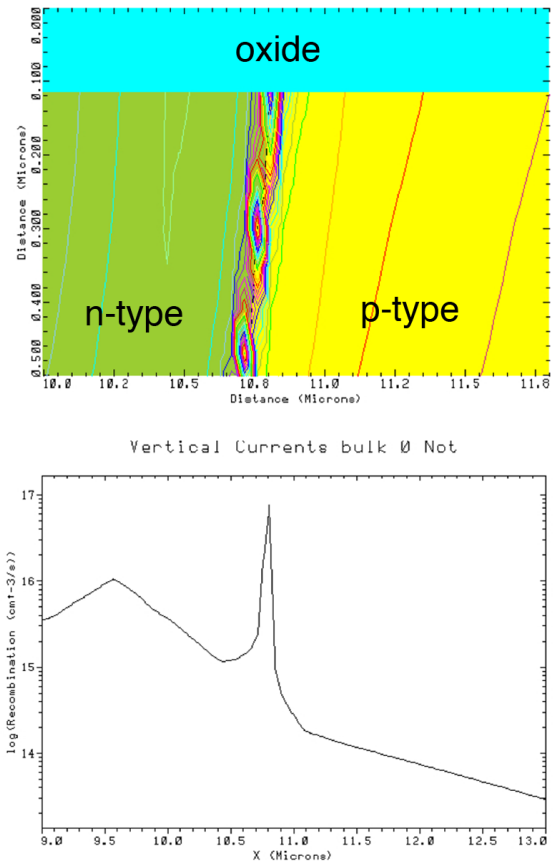

Figure 3.3: (Top) Physical representation of carrier recombination in the base-emitter junction. (Bottom) Cross-section of the recombination current at $y = 2.0\mu m$.

In addition to being maximized in the depletion region, the recombination current is also a function of the base-emitter voltage (V_{BE}). In fact, all three recombination components have a similar variation with V_{BE}. The Gummel-Poon model simplifies the recombination effects in a single exponential term consisting of a composite of all three extra components as:

$$I_{SE}\left(e^{\frac{qV_{BE}}{n_E\,kT}} - 1\right) \tag{3.8}$$

The model parameters are I_{SE} and n_E and are determined by a fit to Equation 3.8. I_{SE} is the non-ideal base-emitter saturation current and n_E is the base-emitter leakage emission coefficient.

Non-ideal Diode Neutron-effects Model Parameters

Recombination effects for a BJT biased in the forward-active region are modeled by Equation 3.8, which require the calibration of two parameters, I_{SE} and n_E. Neutron radiation damage introduces additional lattice defects causing additional recombination current. Using the Gummel-Poon recombination term as a template, the effects of neutron damage were modeled with the exponential term

$$I_{SNEUT}\left(e^{\frac{qV_{BE}}{n_N\,kT}}-1\right) \tag{3.9}$$

Two additional parameters, I_{SNEUT} and n_N, describe the neutron damage effects and were determined from forward-Gummel plots of the BJT test structures at various fluence levels. I_{SNEUT} is the non-ideal base-emitter saturation current after neutron radiation and n_N is the base-emitter leakage emission coefficient after neutron radiation. Both parameters are a function of the fluence and were determined by a linear fit to statistical averages of the data (Figure 3.4).

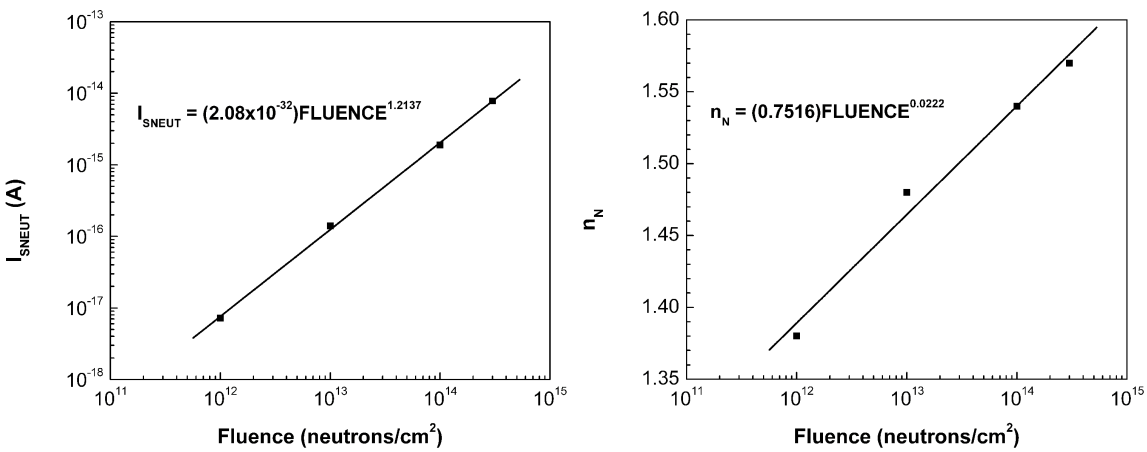

Figure 3.4: Model parameters I_{SNEUT} and n_N as a function of fluence. I_{SNEUT} represents the base-emitter leakage saturation current due to neutrons; n_N represents the base-emitter leakage emission coefficient due to neutrons.

Simulation vs. Measured Data

The "non-ideal diode" term for recombination current due to neutron radiation damage was added to the Gummel-Poon equation for the base current in Verilog-A to get the following:

$$\begin{aligned} I_B &= I_S\left[\frac{1}{\beta_F}\left(e^{\frac{qV_{BE}}{n_F kT}}-1\right)-\frac{1}{\beta_R}\right]+I_{SE}\left(e^{\frac{qV_{BE}}{n_E kT}}-1\right)- \\ & I_{SC}+I_{SNEUT}\left(e^{\frac{qV_{BE}}{n_N kT}}-1\right)+\left(\frac{V_{BE}}{\beta_F}+\frac{V_{BC}}{\beta_R}\right)\mathrm{GMIN} \end{aligned} \tag{3.10}$$

$$\text{where} \qquad I_{SNEUT} = \left(2.08\times 10^{-32}\right)\mathrm{FLU}^{1.2137}$$

$$n_N = (0.7516)\,\mathrm{FLU}^{0.0222}$$

Implementation of this "non-ideal diode" neutron-effects BJT model in SPICE requires an additional model parameter to be specified by the user. The model parameter FLU represents the fluence level ($neutrons/cm^2$) of neutron radiation.

The model was exercised under the same bias conditions used for characterizing the BJT test structures using the forward-gummel test. A comparison of simulated and measured results of the base current as a function of base-emitter voltage at various fluence levels indicate an excellent fit was obtained (Figure 3.5). The measured data were averaged over all devices for each fluence level and there were 12–17 devices at each level. The error bars indicated at $V_{BE} = 0.5\,V$ indicate a 99% confidence interval for the mean value of the base current at that voltage and fluence level. This is a good indication of the spread for the measured data.

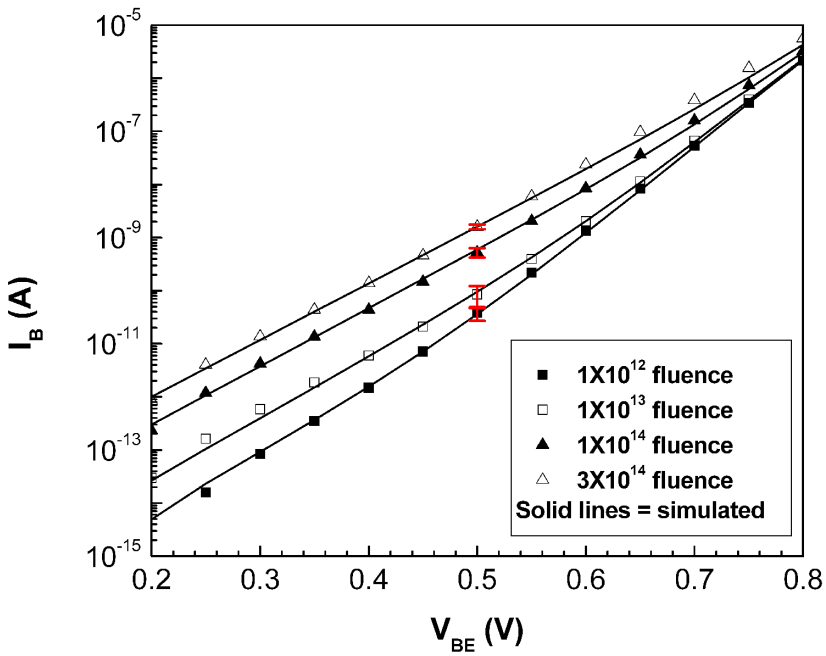

Figure 3.5: Measured and simulated results for NID neutron model.

3.2.2 BJT Model with Neutron Damage Effects: SRH Recombination Equation

Another approach to incorporate static neutron damage effects is to add a term to the base current equation for recombination current described by the SRH theory of recombination. This approach gives more insight into the physical mechanisms that cause BJT current gain degradation. If the dominant contribution to the integral in Equation 3.7 is given by the maximum value of U extending across a portion of the depletion region, the recombination current may be expressed as

$$I_r = \frac{qAx'n_i^2\left(e^{\left(\frac{qV_a}{kT}\right)}-1\right)}{2n_i\left(e^{\left(\frac{qV_a}{2kT}\right)}+1\right)\tau_o}$$

$$I_r \approx \frac{qAx'n_i}{2\tau_o}\exp\left(\frac{qV_a}{2kT}\right) \tag{3.11}$$

In Equation 3.11, $\tau_0 = \frac{1}{N_t \, \sigma \, v_{th}}$ is the lifetime associated with the recombination of excess carriers in a region with a density N_t of recombination centers. For a *npn* BJT, τ_0 is the lifetime of minority carrier electrons in the *p*-type base region.

SRH Neutron-effects Model Parameters

Implementation of the SRH recombination current (Equation 3.11) in a device model is more complicated than implementing the "non-ideal diode" form of an equation because it requires more physical parameters of the device. These parameters are the cross-sectional area of the emitter-base junction (A), the width of the depletion region (x'), the intrinsic doping concentration (n_i), the capture cross-section (σ), and the mean thermal velocity of an electron (v_{th}). In addition, n_i varies with temperature, x' varies with voltage and dopant concentrations and σ is generally determined experimentally for a given type of defect. For the neutron-effects BJT model using the SRH recombination current term, the following assumptions were made [1, 2]:

- A was a tub structure with a flat bottom and curved edges; corners were neglected
- x' was determined assuming an abrupt junction and uniform doping
- n_i varied with temperature as $n_i = \left(9.15 \times 10^{19}\right) \left(\frac{T}{300}\right)^2 e^{-0.5928/kT}$
- $\sigma = 1 \times 10^{-15} \, cm^2$ (typical size for an effective recombination center)
- $v_{th} = 2.3 \times 10^7 cm/s$ (determined for an electron in Si at room temperature)

The density of localized states (N_t) is the parameter that represents the density of defects in the Si lattice. Therefore, N_t has physical significance in determining the current due to recombination. In the SRH neutron-effects BJT model, a parameter N_{tneut} was created to represent the density of defects formed by neutron radiation. Like I_{SNEUT} and n_N, N_{tneut} is a function of fluence and was determined by a linear fit to statistical averages of the data (Figure 3.6).

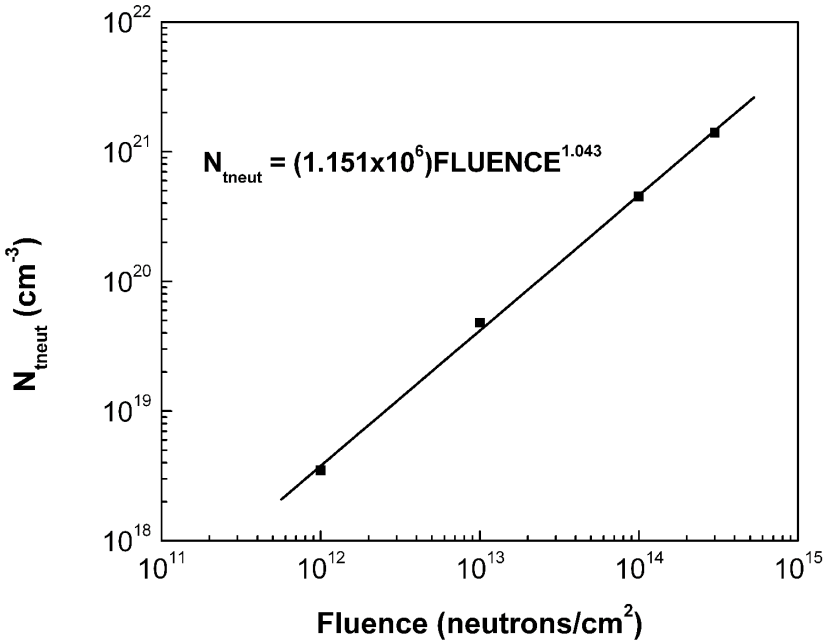

Figure 3.6: Model parameter N_{tneut} as a function of fluence.

For the implementation of the SRH neutron-effects BJT model in Verilog-A, a modification was made to the exponential term in Equation 3.11. A factor of 1.5 was used in the denominator instead of 2 to get

$$I_{NEUT} = \frac{qAx'n_i}{2\tau_o} \exp\left(\frac{qV_a}{1.5\,kT}\right) \tag{3.12}$$

This was done because a factor of 1.5 provided a better fit to the measured data, but the physical meaning of this factor is not yet understood. One possible reason for the discrepancy may be due to bandgap narrowing. High dopant concentrations produce many localized states near the valance and conduction band edges. The density of localized states is so great that it effectively "narrows" the bandgap making it easier for carriers to jump from band to band, which increases the intrinsic carrier concentration. The SRH neutron model does not take bandgap narrowing into account, so the factor of 1.5 may be compensating for this phenomenon.

The SRH term for recombination current due to neutron radiation damage was added to the Gummel-Poon equation for the base current in Verilog-A to get the following:

$$\begin{aligned} I_B &= I_S \left[\frac{1}{\beta_F} \left(e^{\frac{q\,V_{BE}}{n_F\,kT}} - 1 \right) - \frac{1}{\beta_R} \right] + I_{SE} \left(e^{\frac{q\,V_{BE}}{n_E\,kT}} - 1 \right) - \\ & I_{SC} + \frac{qAn_i\,x'}{2\tau_0} \exp\left(\frac{qV_{BE}}{1.5\,kT} \right) + \left(\frac{V_{BE}}{\beta_F} + \frac{V_{BC}}{\beta_R} \right) \text{GMIN} \end{aligned} \tag{3.13}$$

$$\text{where} \qquad \tau_0 = \frac{1}{\left((1.151 \times 10^6)\,\text{FLU}^{1.043} \right) \sigma v_{th}}$$

The additional model parameters required for this model are described in Table 3.2. These model parameters provide the necessary information to calculate the cross-sectional area of the emitter-base junction, the width of the depletion region, and the lifetime of minority carrier electrons in the base.

Table 3.2: SRH Neutron-effects Model Parameters.

Parameter	Description	Units
ϵ_{rsi}	Dielectric constant for silicon	-
N_{coll}	Dopant density of collector	cm^{-3}
N_{base}	Dopant density of base	cm^{-3}
N_{emit}	Dopant density of emitter	cm^{-3}
L_{emit}	Length of the emitter region	m
W_{emit}	Width of the emitter region	m
D_{emit}	Depth of the emitter	m
σ	Electron capture cross section	cm^2
v_{the}	Mean thermal velocity of e- for Si at T=300K	cm/s
FLU	Neutron fluence	$neutrons/cm^2$

A comparison of the simulated and measured results the forward-Gummel test at various fluence levels indicate that the SRH neutron-effects model also obtained an excellent fit (Figure 3.7).

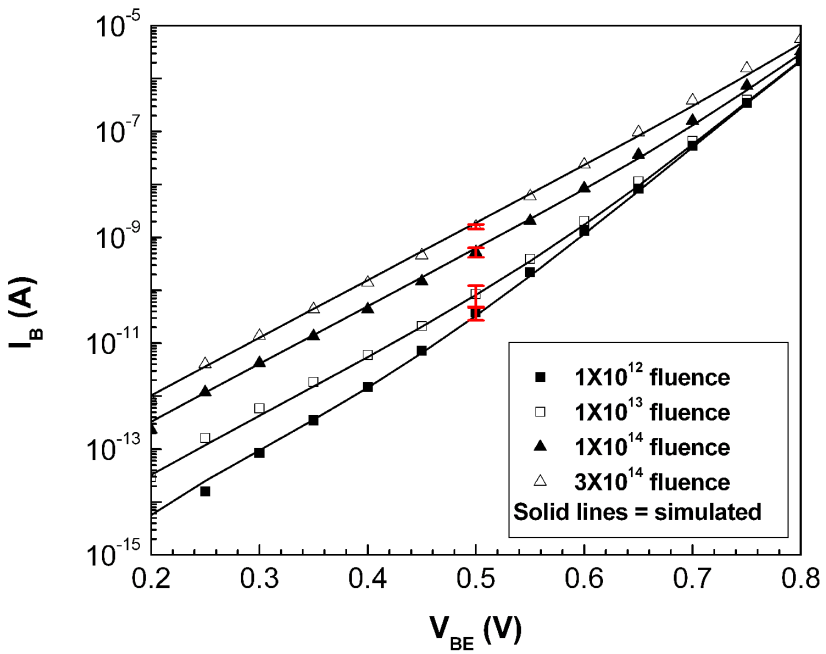

Figure 3.7: Measured and simulated results for the SRH neutron model.

3.2.3 Non-ideal Diode and SRH Neutron Model Comparison

Both the non-ideal diode (NID) and the SRH neutron model were developed to predict the performance of the CMOS6RA BJT after neutron radiation. It is easily seen how neutrons degrade the current gain in Figure 3.8, which shows the current gain (β) with respect to fluence for each model. The mean value of the measured data with a 99% confidence interval is also shown at the indicated fluence levels. The confidence interval indicates 99% confidence that the population mean value of the current gain lies between the lower and upper bounds of the confidence interval. Both models had a current gain with a constant value of 85.3 for fluence levels below $1 \times 10^9\, neutrons/cm^2$ and both indicate a rapid gain degradation from 1×10^{11} to $1 \times 10^{14}\, neutrons/cm^2$. There are slight deviations between the models at those fluence levels, but both models are within the 99% confidence interval. It is not surprising that the simulations lie within the confidence interval since the models

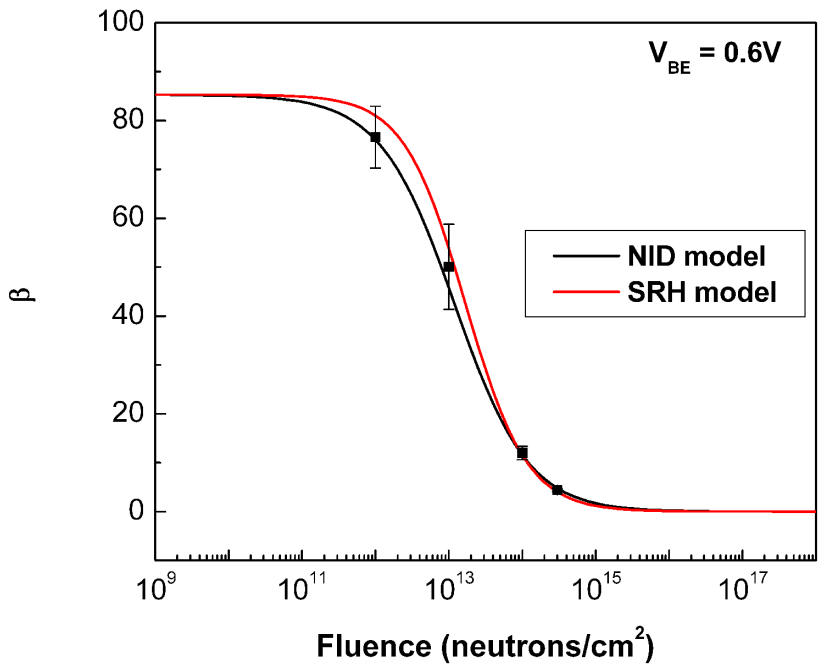

Figure 3.8: Simulation of β degradation with fluence for NID and SRH models.

were developed with the same data. In comparison to the calculated mean value, it appears that the non-ideal diode neutron model predicts the gain degradation with a tighter tolerance. However, there are a number of possibilities that may improve the SRH neutron model. The SRH neutron model is a physics-based description of the recombination of carriers due to neutron radiation. As a result, it is comprised of physical parameters that describe the BJT as well as the energy and type of defects. More accurate values of the parameters that describe the BJT or the inclusion of defects at varying energy levels may improve the predication capability. In addition, the SRH neutron model lends itself to be scaled for different devices with minimal calibration effort. Nevertheless, the non-ideal diode neutron model provides accurate predictive capabilities for this particular device and is relatively easy to understand. It is comprised of a well-known form of equation to describe recombination effects and only requires a single model parameter to be specified. However, it is not easily scalable across devices and requires a great amount of effort to calibrate.

Chapter 4

Example Application

Ultimately, a model's viability depends on it's accuracy of behavior in a simulation of a circuit designed for a specific application. This chapter demonstrates how the neutron BJT model is applied to a voltage reference circuit; the circuit is a generalization of voltage reference circuits used in "real world" applications. Operation of the voltage reference circuit is explained, followed by a discussion of how the circuit was analyzed for neutron radiation performance in the absence of a neutron model. Analysis of the circuit is then carried out with the neutron model to demonstrate the usefulness of the model's predictive capability.

Operation of Voltage Reference

A schematic of the example circuit is shown in Figure 4.1. This is a voltage reference circuit is designed to provide a stable voltage value of 2.5 V over temperature at the VREF node. In this circuit Q1 through Q11 are all identical BJTs. The circuit

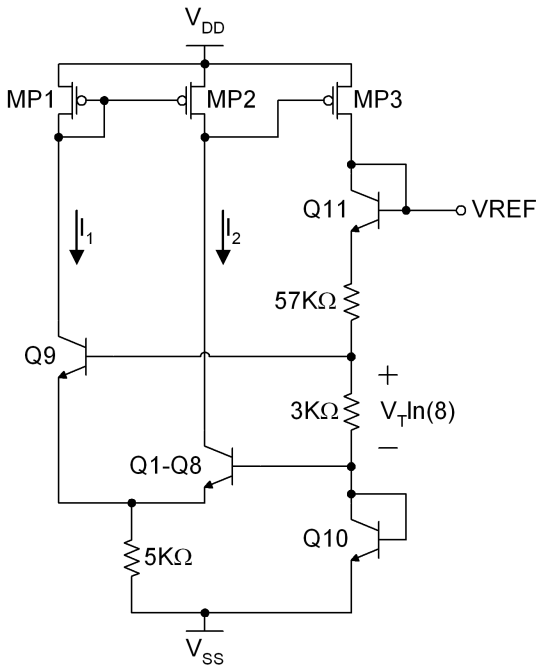

Figure 4.1: Schematic of voltage reference circuit.

works to keep currents I_1 and I_2 equal to insure equal current through Q9 and the parallel combination of Q1 through Q8. Due to the difference in current densities, the resulting voltage across the $3\,K\Omega$ resistor equal to $v_t \ln(8)$, where $v_t = kT/q$ is the thermal voltage and 8 is the ratio of Q9 to Q1-Q8. Differencing of the V_{BE} voltages across that resistor results in a positive temperature coefficient for the $v_t \ln(8)$ voltage. This voltage is summed in series with the V_{BE} voltages of Q10 and Q11, which have negative temperature coefficients. The $57\,K\Omega$ resistor is scaled to achieve a value of $2.5\,V$ at VREF. Thus, the voltage at the VREF node is compensated for temperature.

Analysis of Circuit Without a Neutron Model

To facilitate the development of the voltage reference circuit in a neutron radiation environment, it was designed with a reduced ideal maximum forward current gain parameter (β_F) for the BJTs. This was intentionally done to assure operation of the BJTs with a degraded current gain. Analysis of the voltage reference circuit in a neutron environment was achieved by further reduction of the current gain in a circuit simulation as shown in Figure 4.2. However, this approach did not provide correlation of the current gain degradation to neutron radiation levels and, therefore, makes it difficult to simulate the circuit for neutron radiation specifications.

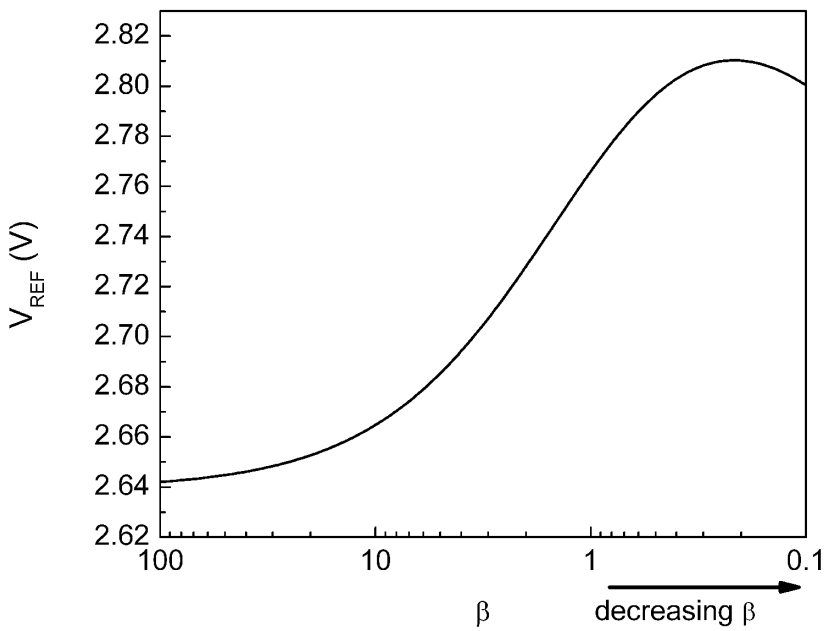

Figure 4.2: Simulation of the voltage reference circuit output (V_{REF}) with respect to current gain (β).

Results of Voltage Reference with Neutron BJT Model

Simulation of the voltage reference circuit with the implementation of the BJT neutron model was performed with a DC sweep of the fluence at a nominal temperature of 27 °C. The output response of V_{REF} is similar to the analysis done without the neutron model as shown in Figure 4.3. However, analysis with the neutron model indicates the output response of V_{REF} with respect to the neutron fluence. Results of the simulation for both approaches to the neutron model are shown. The

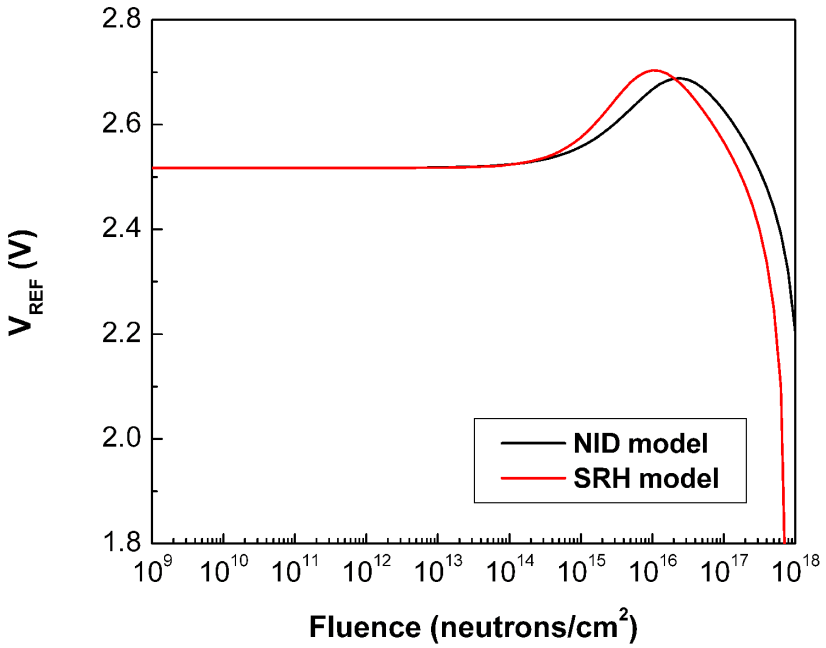

Figure 4.3: Simulation of the voltage reference circuit output (V_{REF}) over fluence.

plot indicates that the circuit begins failure of voltage regulation at a fluence level of $1 \times 10^{15}\, neutrons/cm^2$ and total failure occurs around $6 \times 10^{17}\, neutrons/cm^2$. Again, there are deviations between the two models. However, this type of information is valuable to a circuit designer because it conveys the function of the circuit with respect to neutron fluence levels. In turn, the neutron models allow design of the BJTs with the extracted gain parameter which can help designers achieve tighter tolerances of a circuit.

Chapter 5

Conclusion

It is well known that neutrons affect BJT performance primarily by creating lattice defects, which can dramatically increase carrier recombination rate. In turn, the increase in recombination rate degrades the BJT current gain. This research considered the effects of neutron radiation on the electrical properties of BJTs to develop a compact model for a specific bulk silicon process that can be used in circuit simulators. Two approaches were taken in the development of a model. Both approaches use Verilog-A to add a current component to the Gummel-Poon base current equation. The first approach emulates the Gummel-Poon term for recombination current seen in BJTs under "normal" conditions. The second approach was based on the SRH theory of recombination. Both approaches required model parameters to be defined as a function of fluence. The fluence dependence of the model parameters was determined from measured data of BJT test structures that were exposed to neutron radiation at various fluence levels. Simulation results of the model indicated an excellent fit the the measured data. The model was exercised in a voltage reference circuit, which provided the type of information useful for circuit design in a neutron radiation environment.

Future Work

Although this research provides important circuit design information about a process-specific BJT after neutron radiation, it is not a complete description of BJT operation in a neutron radiation environment. Other regions of operation (i.e. inverse and saturation) and the transient effects of neutron radiation were not considered. Operation of a BJT during a neutron pulse is a major area of study. Consequently, a dynamic compact BJT neutron model is under development at Sandia National Laboratories. The model is being developed to track current gain degradation as a function of time for a variety of bias conditions. It considers various types of defects at various energy levels and the reactions between those defects. The resulting model can then predict transient effects of neutron radiation and be scaled for BJTs fabricated in different processes.

Appendices

Appendix A

Verilog-A BJT Module

```
‘include "discipline.h"
‘include "constants.h"
‘define  REFTEMP    (300.15)
‘define  GMIN       (1.0e-12)

//*******************************************************
//*          Verilog-A/AMS definition of BJT (GP model)
//*                      2003
//*        Based on Berkeley Spice3f5 implementation
//*
//*        This implementation does not account
//*        for excess-phase, and includes substrate
//*******************************************************
//   UPDATED March 8, 19 2004
//      Contributed By: Geoffrey Coram, Ph.D Senior CAD Engineer Analog Devices, Inc.
//   ENHANCED April 16, 2007
//  By: Teresa Gutierrez, Sandia National Laboratories
//   This module is modified to incorporate the effects of neutron fluence on a bjt. Adapted for Sandia’s CMOS6RA process.
//   The model parameters were extracted using IC-CAP from forward gummel data at VC = 2.0V.
//   This bjt module is designed to operate in the forward-active region of operation.

module bjt(C, B, E, S);
   // Function used for voltages limitation
   // external nodes
   inout C, B, E, S;
   electrical C, B, E, S;
   // internal nodes
   electrical ep, bp, cp;
   // BJT type
   // 1 for NPN, -1 for PNP
   parameter integer type=1   from [-1:1];
   // Basic DC parameters
   parameter real is = 1.0e-16;  //[A] transport saturation current
   parameter real bf = 100.0;    //[-] ideal maximum forward beta
   parameter real br = 1.0;        //[-] ideal maximum reverse beta
```

```
parameter real nr = 1.0;        //[-] reverse current emission coefficient
parameter real nf = 1.0;        //[-] forward current emission coefficient
// high current Beta degradation
parameter real ikf = 0.0;    //[A] forward-beta high-current roll-off "knee" current
parameter real ikr = 0.0;   //[A] reverse-beta high-current roll-off "knee" current
parameter real nk  = 0.5;  // [-] knee current roll-off coefficient
// Low current Beta degradation
parameter real ise = 0.0;  //[A] base-emitter leakage saturation current
parameter real ne  = 1.5;  //[-] base-emitter leakage emission coefficient
parameter real isc = 0.0;  //[A] base-collector leakage saturation current
parameter real nc  = 1.5;  //[-] base-collector leakage emission coefficient
// Base width modulation
parameter real var = 0.0;    //[V] reverse Early voltage
parameter real vaf = 0.0;    //[V] forward Early voltage
// Parasitic resistors
parameter real rc  = 1.0e-6   from (0.0:inf);   //[Ohm] collector ohmic resistance
parameter real rb  = 1.0e-6   from (0.0:inf);   //[Ohm] zero-bias (maximum) base resistance
parameter real rbm = 0.0;     //[Ohm] minimum base resistance
parameter real re  = 1.0e-6   from (0.0:inf);  //[Ohm] emitter ohmic resistance
parameter real irb = 0.0;       // [A] current where base resistance equals (rb+rbm)/2   0.0 means infinity
// Junction capacitors
parameter real cje  = 0.0;     //[F] base-emitter zero-bias p-n capacitance
parameter real vje  = 0.75;   //[V] base-emitter built-in potential
parameter real mje  = 0.33;  //[-] base-emitter p-n grading factor
parameter real fc   = 0.5;      //[-] forward-bias depletion capacitor coefficient
parameter real cjc  = 0.0;     //[F] base-collector zero-bias p-n capacitance
parameter real vjc  = 0.75;   //[V] base-collector built-in potential
parameter real mjc  = 0.33;  //[-] base-collector p-n grading factor
parameter real xcjc = 0.0;    //[-] fraction of CBC connected internal to RB
parameter real cjs  = 0.0;     // [F] zero bias substrate junction capacitance
parameter real vjs  = 0.75;    // [V] substrate junction built in potential
parameter real mjs  = 0.33;   //[-] substrate junction exponential factor
// Substrate current
parameter real iss = 0.0;    // [A] base-substrate saturation current
parameter real ns  = 1.0;   // substrate current emission factor
// Transit time
parameter real tf  = 0.0;    //[s] ideal reverse transit time
parameter real xtf = 0.0;   //[-] transit time bias dependence coefficient
parameter real itf = 0.0;    //[A] transit time dependency on IC
parameter real vtf = 0.0;   //[V] transit time dependency on VCB
parameter real tr  = 0.0;    //[s] ideal reverse transit time
// Temperature effects
parameter real xtb = 0.0;      // [-] forward and reverse beta temperature exponent
parameter real eg  = 1.16;   //[eV] badgap voltage (barrier height)
parameter real xti = 3.0;       // [-] temperature exponent for is
parameter real tnom  = 300.15;  //[K] nominal temperature
//(at which all input data is assumed to have been measured)
//*********************************************************************************************
// The following parameter was added for the neutron-effects BJT model: non-ideal diode eqn.
parameter real flu = 3.0e14;     // [neutrons/cm^2] Neutron fluence
//*********************************************************************************************
// The following parameters were added for the neutron-effects BJT model
// using the SRH recombination equation
// Material constants and geometery of device
parameter real ersi = 11.68; //[-] dielectric constant for silicon
parameter real ncoll = 4.0e17; //[cm^-3] dopant density of the collector
parameter real nbase = 1.0e18; //[cm^-3] dopant density of the base
parameter real nemit = 1.0e20;  //[cm^-3] dopant density of the emitter
```

```
   parameter real ngrade = 1.5; //[-] grade of the junction; 2=step junction
   parameter real elength = 2.0e-6; //[m] length of the emitter region
   parameter real ewidth = 2.0e-6; //[m] width of the emitter region
   parameter real edepth = 2.0e-7; //[m] depth of the emitter region
   // Neutron effects
   parameter real flu = 3.0e14;     // [neutrons/cm^2] Neutron fluence
   parameter real sigma = 1.0e-15; //[cm^2] electron capture cross section
   parameter real vthe = 2.30e7; //[cm/s] mean thermal velocity of an electron for Si at T=300K

   //*****************************************************************************
   // Variables for bias voltages
   real            vbe, vbx, vbc, vce, vcs;
   // Variables for temperature scaling
   real            fact2, egfet, arg, pbfact, ratlog,
     ratio1, factlog, factor, bfactor,
     pbo, gmaold, gmanew, fact1;
   real             tis, tbf, tbr, tise, tisc,
     tcje, tvje, tcjc, tvjc, tDepCap,
     xfc, f2, f3, f6, tf1, tf4, tf5;
   // Variables for currents/charges computation
   real             vtn, vte, vtc,
     evbe, cbe, evben, cben,
     evbc, cbc, evbcn, cbcn,
     cre, crc, crb, rx,
     inv_var, inv_vaf;
   real             ovtf, q1, q2, qb, sqarg,
     argtf, arg1, arg2, sarg,
     temp, czbef2, czbcf2,
     czbxf2, cb, cc, czbc, czbx,
     qbe, qbc, qbx, qcs;
   //*************************************************************************************************
   // The following variables were added for the neutron-effects BJT model: non-ideal diode eqn.
   real iseneut, nfneut, vtneut, eneut, cneut;
   //*************************************************************************************************
   // The following variables were added for the neutron-effects BJT model: SRH recombination eqn.
   real esi, ni, ncoll_m, nbase_m, nemit_m, bedopants, bevbi,
        esarea, ntneut, tauneut, xd, qAni, cneut;
   //*************************************************************************************************
  analog
     begin
// Temperature scaling and constants initialization
        xfc = ln(1.0 - fc);
        f2 = exp((1.0 + mje) * xfc);
        f3 = 1.0 - fc * (1.0 + mje);
        f6 = exp((1.0 + mjc)*xfc);
if (vaf != 0.0)
  inv_vaf = 1.0 / vaf;
else
  inv_vaf = 0.0;
if (var != 0.0)
  inv_var = 1.0 / var;
else
  inv_var = 0.0;
        fact1 = tnom/`REFTEMP;
        fact2 = $temperature/`REFTEMP;
        egfet = 1.16-(7.02e-4*$temperature*$temperature)/($temperature+1108.0);
        arg = -egfet/(2.0*`P_K*$temperature)+1.1150877/(`P_K*(`REFTEMP+`REFTEMP));
        pbfact = -2.0*$vt*(1.5*ln(fact2)+`P_Q*arg);
```

```
        ratlog = ln($temperature/tnom);
        ratio1 = $temperature/tnom -1;
        factlog = ratio1 * eg/$vt + xti*ratlog;
        factor = exp(factlog);
        tis = is * factor;
        bfactor = exp(ratlog*xtb);
        tbf = bf * bfactor;
        tbr = br * bfactor;
        tise = ise * exp(factlog/ne)/bfactor;
        tisc = isc * exp(factlog/nc)/bfactor;
        pbo = (vje-pbfact)/fact1;
        gmaold = (vje-pbo)/pbo;
        tcje = cje/(1+mje*(4e-4*(tnom-`REFTEMP)-gmaold));
        tvje = fact2 * pbo+pbfact;
        gmanew = (tvje-pbo)/pbo;
        tcje = tcje * (1+mje*(4e-4*($temperature-`REFTEMP)-gmanew));
        pbo = (vjc-pbfact)/fact1;
        gmaold = (vjc-pbo)/pbo;
        tcjc = cjc/(1+mjc*(4e-4*(tnom-`REFTEMP)-gmaold));
        tvjc = fact2 * pbo+pbfact;
        gmanew = (tvjc-pbo)/pbo;
        tcjc = tcjc * (1+mjc*(4e-4*($temperature-`REFTEMP)-gmanew));
        tDepCap = fc * tvje;
        tf1 = tvje * (1.0 - exp((1.0 - mje) * xfc)) / (1.0 - mje);
        tf4 = fc * tvjc;
        tf5 = tvjc * (1.0 - exp((1.0 - mjc) * xfc)) / (1.0 - mjc);
        //*********************************************************************************
        // Initialization of variables for neutron-effects BJT model: SRH recombination eqn.
    esi = `P_EPS0*ersi; //static permittivity of silicon
    ni = 9.15e19*pow(`REFTEMP/300,2)*exp(-0.5928/$vt); //intrinsic carrier concentraion [cm^-3]
    ncoll_m = ncoll*pow(100,3); //dopant density of collector in m^-3
    nbase_m = nbase*pow(100,3); //dopant density of base in m^-3
    nemit_m = nemit*pow(100,3); //dopant density of emitter in m^-3
    // bedopants = nbase*nemit/pow(ni,2);  //using Maxwell-Boltzman statistics
    bedopants = nbase/ni; //for high dopant concentrations Na or Nd >= 1X10^19 [cm^-3]
    bevbi =0.56 + $vt*ln(bedopants); //built-in voltage at base-emitter junction
    esarea = elength*ewidth + (elength+ewidth)*`M_PI*edepth + (`M_PI*pow(edepth,2))/2; //emitter surface area
    qAni = `P_Q*esarea*ni;
    //*********************************************************************************************
// Get external bias voltages
vbe = type * V(bp, ep);
vbc = type * V(bp, cp);
vcs = type * V(S,  cp);
vbx = type * V(B,  cp);
// Equations computation start here
        vte = ne*$vt;
        vtc = nc*$vt;
  vtn=$vt*nf;
        if (vbe > -5.0*vtn)
  begin
            evbe=exp(vbe/vtn);
            cbe=tis*(evbe-1.0) + `GMIN*vbe;
            //*************************************************************************
            // Equations added for neutron-effects BJT model: non-ideal diode eqn.
            iseneut=2e-32*pow(flu,1.2137);
            nfneut=0.7516*pow(flu,0.0222);
            vtneut=$vt*nfneut;
            eneut=exp(vbe/vtneut);
```

```
            cneut=iseneut*(eneut-1.0);
            //*******************************************************************************
            // Equations added for neutron-effects BJT model: SRH recombination eqn.
            xd = sqrt(2*esi/`P_Q*(1/nbase_m+1/nemit_m)*(bevbi-vbe)); //depletion width for an abrupt pn junction
            ntneut = 1.151212e6*pow(flu,1.043063);
            tauneut = 1/(ntneut*vthe*sigma);
            cneut = (qAni*xd/(2*tauneut))*exp(vbe/(ngrade*$vt));
            //*******************************************************************************
            if (tise == 0)
              cben=0;
    else
      begin
                evben=exp(vbe/vte);
                cben=tise*(evben-1);
      end
         end
else
  begin
            cbe = -tis + `GMIN*vbe;
            cben= -tise;
         end // else: !if(vbe > -5.0*vtn)
       vtn=$vt*nr;
       if (vbc > -5.0*vtn)
  begin
            evbc=exp(vbc/vtn);
            cbc=tis*(evbc-1) + `GMIN*vbc;
            if (tisc == 0)
              cbcn=0;
    else
      begin
                evbcn=exp(vbc/vtc);
                cbcn=tisc*(evbcn-1);
            end
         end
  else
  begin
            cbc = -tis + `GMIN*vbc;
            cbcn= -tisc;
         end // else: !if(vbc > -5.0*vtn)
       /*
        *   determine base charge terms
        */
       q1=1/(1-inv_vaf*vbc-inv_var*vbe);
       if (ikf == 0 && ikr == 0)
         qb=q1;
else
  begin
            q2=cbe/ikf+cbc/ikr;
            arg=max(0,1.0+4*q2);
            sqarg=1;
            if (arg != 0) sqarg=sqrt(arg);
            qb=q1*(1+sqarg)/2.0;
         end // else: !if(ikf == 0 && ikr == 0)
       /*
        *   determine dc incremental conductances
        */
       cc=(cbe-cbc)/qb-cbc/tbr-cbcn;
       cb=cbe/tbf+cben+cbc/tbr+cbcn;
```

```
        //*********************************************************************************************************
        // Equation for cb used for neutron-effects BJT model: non-ideal diode eqn. & SRH recombination eqn.
        cb=cbe/tbf+cben+cbc/tbr+cbcn+cneut;
        //*********************************************************************************************************
// Resistors
cre = V(E, ep) / re;
crc = V(C, cp) / rc;
rx = rb + (rb-rbm)/qb;
if (irb != 0.0)
  begin
     arg1=max(cb/irb,1e-9);
                     arg2=(-1.0 + sqrt(1+14.59025*arg1))/2.4317/sqrt(arg1);
                     arg1=tan(arg2);
                     rx=rb+3.0*(rb-rbm)*(arg1-arg2)/arg2/arg1/arg1;
  end
crb = V(B, bp) / rx;
        /*
         *   charge storage elements
         */
if (analysis("tran", "ac"))
  begin
             czbc=cjc*xcjc;
             czbx=cjc-czbc;
     if (vtf != 0.0)
               ovtf = 1.0 / (vtf*1.44);
     else
       ovtf = 0.0;
             if(tf != 0 && vbe >0)
       begin
                 argtf=0;
                 arg2=0;
                 if(xtf != 0)
    begin
       argtf=xtf;
       if (ovtf != 0)
 argtf=argtf*exp(vbc*ovtf);
                      arg2=argtf;
                      if (itf != 0)
 begin
                           temp=cbe/(cbe+itf);
                           argtf=argtf*temp*temp;
                           arg2=argtf*(3.0  -temp - temp);
                         end
                    end
                 cbe=cbe*(1+argtf)/qb;
               end
             if (vbe < tDepCap)
       begin
                 arg=1-vbe/tvje;
                 sarg=exp(-mje*ln(arg));
                 qbe=tf*cbe+tvje*tcje*(1-arg*sarg)/(1-mje);
               end
     else
       begin
                 czbef2=tcje/f2;
                 qbe = tf*cbe+tcje*tf1+czbef2*
                        (f3*(vbe-tDepCap) +(mje/(tvje+tvje))*(vbe*vbe-tDepCap*tDepCap));
             end // else: !if(vbe < tDepCap)
```

```
            if (vbc < tf4)
       begin
                arg=1-vbc/tvjc;
                sarg=exp(-mjc*ln(arg));
                qbc = tr*cbc+tvjc*czbc*(1-arg*sarg)/(1-mjc);
              end
     else
       begin
                czbcf2=czbc/f6;
                qbc = tr*cbc+czbc*tf5+czbcf2*
                       (f3*(vbc-tf4) +(mjc/(tvjc+tvjc))*(vbc*vbc-tf4*tf4));
              end // else: !if(vbc < tf4)
            if (vbx < tf4)
       begin
                arg=1-vbx/tvjc;
                sarg=exp(-mjc*ln(arg));
                qbx = tvjc*czbx* (1-arg*sarg)/(1-mjc);
              end
     else
       begin
                czbxf2=czbx/f6;
                qbx=czbx*tf5+czbxf2*
                    (f3*(vbx-tf4)+(mjc/(tvjc+tvjc))*(vbx*vbx-tf4*tf4));
              end // else: !if(vbx < tf4)
            if (vcs < 0)
       begin
                arg=1-vcs/vjs;
                sarg=exp(-mjs*ln(arg));
                qcs = vjs*cjs*(1-arg*sarg)/(1-mjs);
              end
     else
              qcs = vcs*cjs*(1+mjs*vcs/(2*vjs));
  end // if (analysis("tran", "ac"))
else
  begin
     qcs = 0.0;
     qbx = 0.0;
     qbc = 0.0;
     qbe = 0.0;
  end
// Current equations
I(E,  ep) <+ cre;
I(C,  cp) <+ crc;
I(B,  bp) <+ crb;
I(cp, ep) <+ type * cc;
I(bp, ep) <+ type * cb;
// Charges equations
I(S,  cp) <+ type * ddt (qcs);
I(B,  cp) <+ type * ddt (qbx);
I(bp, cp) <+ type * ddt (qbc);
I(bp, ep) <+ type * ddt (qbe);
     end
endmodule
```

Appendix B

Model Parameters

Table B.1: Gummel-Poon Model Parameters

Parameter	Description	Value
BF	Ideal Maximum Forward Beta	91.61
BR	Ideal Maximum Reverse Beta	1
CJC	Base-collector Zero-bias p-n Capacitance (farad)	0
CJE	Base-emitter Zero-bias p-n Capacitance (farad)	0
CJS	Substrate Zero-bias p-n Capacitance (farad)	0
EG	Bandgap Voltage (Barrier Height) (eV)	1.11
FC	Forward-bias Depletion Capacitor Coefficient	0.5
IKF	Corner for Forward-beta High-current Roll-off (amp)	1.654E-03
IKR	Corner for Reverse-beta High-current Roll-off (amp)	10
IRB	Current at which Rb Falls off by half (amp)	2.46E-06
IS	Transport Saturation Current (amp)	7.596E-18
ISC	Base-collector Leakage Saturation Current (amp)	0
ISE	Base-emitter Leakage Saturation Current (amp)	3.843E-17
ITF	Transit Time Dependency on Ic (amp)	0
KF	Flicker Noise Coefficient	0
MJC	Base-collector p-n Grading Factor	0.333
MJE	Base-emitter p-n Grading Factor	0.333
MJS	Substrate p-n Grading Factor	0
NC	Base-collector Leakage Emission Coefficient	2
NE	Base-emitter Leakage Emission Coefficient	1.599
NF	Forward Current Emission Coefficient	0.9985
NK	High Current Roll-off Coefficient	0.5
NR	Reverse Current Emission Coefficient	1
PTF	Excess Phase @ 1/(2 TF)Hz (degree)	0
RB	Zero-bias (Maximum) Base Resistance (ohm)	533
RBM	Minimum Base Resistance (ohm)	44.77
RC	Collector Ohmic Resistance (ohm)	64.41
RE	Emitter Ohmic Resistance (ohm)	3.9
TF	Ideal Forward Transit Time (sec)	0
TR	Ideal Reverse Transit Time (sec)	1.00E-09
TNOM	Parameter Measurement Temperature (C)	27
VAF	Forward Early Voltage (volt)	1000
VAR	Reverse Early Voltage (volt)	1000
VJC	Base-collector Built-in Potential (volt)	0.75
VJE	Base-emitter Built-in Potential (volt)	0.75
VJS	Substrate Built-in Potential (volt)	0.75
VTF	Transit Time Dependency on Vbc (volt)	1000
XCJC	Fraction of CJC Connected Internally to RB	1
XTB	Forward and Reverse Beta Temperature Coefficient	0
XTF	Transit Time Bias Dependence Coefficient	0

Table B.2: Non-Ideal Diode Additional Model Parameters

Parameter	Description	Value
FLU	Fluence level ($neutrons/cm^2$)	1

Table B.3: SRH Additional Model Parameters

Parameter	Description	Value
ERSI	dielectric constant for silicon	11.68
NCOLL	dopant density of the collector [cm^{-3}]	4.0e17
NBASE	dopant density of the base [cm^{-3}]	1.0e18
NEMIT	dopant density of the emitter [cm^{-3}]	1.0e20
NGRADE	grade of the junction	1.5
ELENGTH	length of the emitter region [m]	2.0e-6
EWIDTH	width of the emitter region [m]	2.0e-6
EDEPTH	depth of the emitter region [m]	2.0e-7
FLU	neutron fluence [$neutrons/cm^2$]	1
SIGMA	electron capture cross section [cm^2]	1.0e-15
VTHE	mean thermal velocity of an electron [cm/s]	2.30e7

References

[1] R. S. Muller and T. I. Kamins. *Device Electronics for Integrated Circuits*. John Wiley, New York, second edition, 1986.

[2] R. F. Pierret. *Semiconductor Device Fundamentals*. Addison-Wesley, Reading, MA, USA, 1996.

[3] D. A. Neamen. *Semiconductor Physics & Devices: Basic Principles*. Irwin, Chicago, second edition, 1997.

[4] W. Shockley and W. T. Read. Statistics of the recombinations of holes and electrons. *Phys. Rev.*, 87(5):835–842, September 1952.

[5] R. N. Hall. Electron-hole recombination in germanium. *Phys. Rev.*, 87(2):387, July 1952.

[6] J. J. Ebers and J. L. Moll. Large signal behavior of junction transistors. *Proc. IEEE*, 42, 1954.

[7] H. K. Gummel and H. C. Poon. An integral charge control model of bipolar transistors. *The Bell System Technical Journal*, 49:827–852, May 1970.

[8] J. R. Srour, C. J. Marshall, and P. W. Marshall. Review of displacement damage effects in silicon devices. *IEEE Transactions on Nuclear Science*, 50(3):653–670, June 2003.

[9] F. Larin. *Radiation Effects in Semiconductor Devices*. John Wiley, New York, 1968.

[10] G. C. Messenger and M. S. Ash. *The Effects of Radiation on Electronic Systems*. Van Nostrand Reinhold, New York, second edition, 1992.

[11] B. L. Gregory. Minority carrier recombination in neutron irradiated silicon. *IEEE Transactions on Nuclear Science*, 16:53–62, December 1969.

[12] J. W. Easley and J. A. Dooley. On the neutron bombardment reduction of transistor current gain. *Journal of Applied Physics*, 31(6):1024–1028, June 1960.

[13] C. A. Goben. A study of the neutron-induced base current component in silicon transistors. *IEEE Transactions on Nuclear Science*, 12:134–146, October 1965.

[14] C. A. Goben, F. M. Smits, and J. L. Wirth. Neutron radiation damage in silicon transistors. *IEEE Transactions on Nuclear Science*, 15:1429, April 1968.

[15] M. Frank and C. D. Taulbee. Factors influencing prediction of transistor current gain in neutron radiation. *IEEE Transactions on Nuclear Science*, 14:127–133, December 1967.

[16] G. C. Messenger. Current gain degradation due to displacement damage for graded base transistors. *Proc. IEEE*, 55:413–414, March 1967.

[17] G. C. Messenger. A general proof of the beta degradation equation for bulk displacement damage. *IEEE Transactions on Nuclear Science*, 20:809–810, February 1973.

[18] C. A. Goben and F. M. Smits. Anomalous base current component in neutron-irradiated transistors. Sand Report SC-R-64-195, Sandia National Laboratories, July 1964.

[19] H. S. Hajghassem, J. R. Yeargan, and W. D. Brown. Modelling the effects of neutron radiation on the gummel-poon parameters for bipolar npn transistors. *Microelectron. Reliab.*, 31(5):969–984, 1991.

[20] Y. Deng, T. A. Fjeldly, T. Ytterdal, and M. S. Shur. Spice modeling of neuton displacement damage and annealing effects in bipolar junction transistors. *IEEE Transactions on Nuclear Science*, 50(6):1873–1877, December 2003.

[21] J. J. Liou, J. S. Yuan, and H. Shakouri. Modulating the bipolar junction transistor subjected to neutron irradiation for integrated circuit simulation. *IEEE Transactions on Electron Devices*, 39(3):593–597, March 1992.

[22] K. Kundert and O. Zinke. *The Designer's Guide to Verilog-AMS*. Springer, first edition, 2004.

[23] F. Sischka. Gummel-poon bipolar model: model description, parameter extraction. Technical report, Agilent Technologies, April 2002.

[24] I. Getreu. *Modeling the Bipolar Transistor*. Tektronix, 1976.

[25] G. Massobrio and P. Antognetti. *Semiconductor Device Modeling with SPICE*. McGraw-Hill, second edition, 1993.

[26] C. E. Hembree. Study of oxide traps on recombination current in 2n222 bipolar junction transistors. Unpublished Sandia Report, 2007.